© 2022. Published by The Company of Biologists Ltd | Development (2022) 149, dev200465. doi:10.1242/dev.200465

RESEARCH ARTICLE

The germ plasm is anchored at the cleavage furrows through interaction with tight junctions in the early zebrafish embryo

Nadia Rostam[1,2,*,‡], Alexander Goloborodko[3], Stephan Riemer[3], Andres Hertel[4], Dietmar Riedel[5], Gerd Vorbrüggen[2,4] and Roland Dosch[1,3]

ABSTRACT

The zebrafish germline is specified during early embryogenesis by inherited maternal RNAs and proteins collectively called germ plasm. Only the cells containing germ plasm will become part of the germline, whereas the other cells will commit to somatic cell fates. Therefore, proper localization of germ plasm is key for germ cell specification and its removal is crucial for the development of the soma. The molecular mechanism underlying this process in vertebrates is largely unknown. Here, we show that germ plasm localization in zebrafish is similar to that in *Xenopus* but distinct from *Drosophila*. We identified non muscle myosin II (NMII) and tight junction (TJ) components, such as ZO2 and claudin-d (Cldn-d) as interaction candidates of Bucky ball (Buc), which is the germ plasm organizer in zebrafish. Remarkably, we also found that TJ protein ZO1 colocalizes with germ plasm, and electron microscopy of zebrafish embryos uncovered TJ-like structures at the cleavage furrows where the germ plasm is anchored. In addition, injection of the TJ receptor Cldn-d produced extra germ plasm aggregates, whereas expression of a dominant-negative version inhibited germ plasm aggregate formation. Our findings support for the first time a role for TJs in germ plasm localization.

KEY WORDS: Germ plasm localization, Zebrafish, Tight junctions, Bucky ball, ZO proteins, Claudin-d

INTRODUCTION

Germ plasm consists of a maternally inherited ribonucleo-protein (RNP) condensate, which controls the formation of the germline in many animals (Strome and Updike, 2015; Aguero et al., 2017). Germ plasm thereby acts as a classical cytoplasmic determinant during embryonic development with the following activities: (1) in the zygote, germ plasm is uniformly distributed and, after the cleavage, period leads to the formation of a subpopulation of embryonic cells containing germ plasm; (2) these cells will be programmed to differentiate into primordial germ cells (PGCs), while the other cells without germ plasm adopt a somatic fate, e.g. neuron, muscle, etc. Proper segregation of germ plasm allows its accumulation in presumptive PGCs, whereas it is subsequently degraded in prospective somatic cells.

The germ plasm specification of PGCs seem to be largely conserved during evolution, because many components like Vasa, Nanos and Piwi are present throughout most animal genomes (Ewen-Campen et al., 2010; Juliano et al., 2010). By contrast, it is currently unknown whether the molecular mechanisms controlling localization of germ plasm are also conserved during evolution.

The positioning of germ plasm during embryogenesis is best understood in invertebrates, because of their powerful molecular-genetic tools. In *C. elegans*, the entry of sperm determines embryonic polarity (Otto and Goldstein, 1992; Strome and Wood, 1983), which eventually leads to asymmetric localization of germ plasm and germline specification (Seydoux, 2018; Strome and Updike, 2015). In the fly *Drosophila*, local translation of the germ plasm organizer Oskar (Osk) recruits germ plasm components to the cellular cortex of the posterior pole (Ephrussi and Lehmann, 1992; Kim-Ha et al., 1993; Trcek and Lehmann, 2019). Among vertebrates using germ plasm for germline specification, some key discoveries of its localization were made in the frog *Xenopus laevis* (Houston, 2013; Aguero et al., 2017). In *Xenopus laevis* it was shown that during oogenesis germ plasm first accumulates at the prominent Balbiani body (BB), also called mitochondrial cloud (Heasman et al., 1984). Germ plasm then becomes anchored at the vegetal pole and after fertilization is passively inherited during the cleavage period of the most vegetal blastomeres (Ressom and Dixon, 1988; Aguero et al., 2017). At the blastula stage, germ plasm-positive cells internalize into the embryo and then start their migratory journey until they reach the gonads. However, the molecular structure tethering germ plasm to the vegetal pole during the cleavage period of *Xenopus* embryogenesis is not known.

In zebrafish egg, germ plasm also initially accumulates at the BB and subsequently localizes to the vegetal pole, as in *Xenopus* (Dosch, 2015; Moravec and Pelegri, 2020; Raz, 2003). However, in contrast to *Xenopus*, after fertilization, germ plasm streams together with cytoplasm during 'ooplasmic segregation' into the forming blastodisc at the animal pole of the zebrafish embryo (Welch and Pelegri, 2014). Subsequently, germ plasm localizes to the cleavage furrows at the four-cell stage, forming four aggregates in close proximity to the apical ends of the furrows (Olsen et al., 1997; Raz, 2003; Yoon et al., 1997). Indeed, maternal mutants affecting the first embryonic cleavages also interfere with germ plasm recruitment (Nair et al., 2013; Yabe et al., 2007). The first described cytoskeletal structure tethering germ plasm in zebrafish was described as a furrow-associated microtubule array (FMA) (Jesuthasan, 1998; Pelegri et al., 1999). However, the FMA starts to disassemble after the third cleavage, leaving the molecular identity

[1]Institute of Human Genetics, University Medical Center, 37073 Göttingen, Germany. [2]Department of Developmental Biology, Johann-Friedrich-Blumenbach Institute of Zoology and Anthropology, Göttingen Center of Molecular Biosciences, University of Göttingen, 37077 Göttingen, Germany. [3]Institute for Developmental Biochemistry, University Medical Center, 37077 Göttingen, Germany. [4]Department of Molecular Developmental Biology, Max Planck Institute for Biophysical Chemistry, 37077 Göttingen, Germany. [5]Laboratory of Electron Microscopy, Max Planck Institute for Biophysical Chemistry, 37077 Göttingen, Germany. *Present address: Max Planck Institute of Molecular Cell Biology and Genetics, Pfotenhauerstrasse 108, 01307 Dresden, Germany.

‡Author for correspondence (rostam@mpi-cbg.de)

N.R., 0000-0002-6891-594X; A.G., 0000-0002-5028-5572; S.R., 0000-0003-2371-2724; A.H., 0000-0002-0608-0174; D.R., 0000-0003-2970-6894; R.D., 0000-0001-9247-8586

Handling Editor: Swathi Arur
Received 12 January 2022; Accepted 6 June 2022

Development (2022) 149, dev200465. doi:10.1242/dev.200465

of the cellular structure anchoring germ plasm after the eight-cell stage unresolved. A role for cytoskeletal structure for germ plasm transport is further supported by the observation that inhibitors for Rho and Rock activity, which are enriched at the cleavage furrows at the four-cell stage, affect cytoskeletal structures and result in additional mislocalized germ plasm aggregates (Miranda-Rodríguez et al., 2017).

Molecular and genetic screens identified the proteins that are specifically localized to these four germ plasm spots, e.g. zebrafish Piwi (Ziwi) (Houwing et al., 2007), phosphorylated non muscle myosin II (p-NMII) (Nair et al., 2013) and Bucky ball (Buc) (Bontems et al., 2009; Campbell et al., 2015; Riemer et al., 2015; Roovers et al., 2018). Buc appears to exert a central role during germline specification, because it acts as a germ plasm organizer by recruiting other germ plasm components and thereby triggers germline specification (Bontems et al., 2009; Heim et al., 2014; Krishnakumar et al., 2018; Marlow and Mullins, 2008). Buc interacts through Kinesin Kif5Ba with microtubules, which is essential for Buc transport towards the cleavage furrows (Campbell et al., 2015). However, it is not clear which cellular structure anchors Buc after its transport to the four germ plasm spots in the early embryo.

Here, we show that the germ plasm nucleators Buc and its *Xenopus* homolog Velo1 use conserved mechanisms for their anchorage, whereas *Drosophila* Osk localizes by a distinct mode. We mapped the localization motif in the Buc protein and used the isolated peptide to purify its interactors from zebrafish embryos. Among numerous proteins, we identified subunits of the NMII complex, which is a known cytoskeletal component of adherens junctions, tight junctions and midbodies (Liu et al., 2012; Vicente-Manzanares et al., 2009). In addition, ZO2 and the adherence receptor of tight junctions claudin-d (Cldn-d) were identified to be associated with the Buc localization domain. Furthermore, we discovered that TJ protein ZO1 colocalizes with the four germ plasm aggregates at the cleavage furrows at the eight-cell stage. Electron microscopy (EM) of zebrafish embryos uncovered TJ-like structures at the cleavage furrows that are in proximity to germ plasm at the eight-cell stage. Moreover, overexpressing the tight junction receptor Cldn-d led to the formation of ectopic germ plasm aggregates in zebrafish embryos. Taken together, our results identify TJs as the cellular structures that recruit germ plasm at the onset of zebrafish embryogenesis.

RESULTS

Zebrafish Buc and *Xenopus* Velo1 localize similarly in zebrafish embryos

Consistent with its function as a germ plasm organizer, Buc localizes to the germ plasm throughout early embryogenesis (Bontems et al., 2009; Heim et al., 2014; Riemer et al., 2015). To address whether this localization mechanism is conserved between zebrafish and *Xenopus*, we injected mRNA encoding GFP-fusions of these germ plasm organizers into one-cell zebrafish embryos (Fig. 1A). At 2.5-3 h post fertilization (hpf), we analysed whether the GFP-fusion proteins colocalized with the germ plasm using an antibody against the endogenous Buc protein, which is tightly associated with the germ plasm (Riemer et al., 2015), and an antibody detecting β-catenin to label the membrane of the cleavage furrows. Western blot of *in vitro* translated proteins confirmed the specificity of the Buc antibody (Fig. S1). Injections of mRNA encoding Buc-GFP colocalized with zebrafish germ plasm, recapitulating the positioning of the germ plasm (Fig. 1B,C, Fig. S2A) (Bontems et al., 2009). Similarly, Velo1-GFP colocalized with the germ plasm (Fig. 1B,D, Fig. S2B), suggesting that zebrafish Buc and *Xenopus* Velo1 are targeted by a similar molecular machinery for germ plasm recruitment.

To test whether the localization mechanism also detects the invertebrate germ plasm organizer short Osk, mRNA of sOsk fused to GFP was also injected. In contrast to Buc and Velo1, sOsk-GFP did not overlap with the germ plasm in injected zebrafish embryos (Fig. 1B, Fig. S2C), but instead localized to the nuclei, as previously shown in insect cells and in *Drosophila* embryos (Jeske et al., 2017; Kistler et al., 2018), similar to control injections of a GFP that resulted in a ubiquitous subcellular localization, including the nucleus (Fig. 1B,E, Fig. S2C,D). These results suggest that the recruitment machineries of germ plasm in zebrafish and *Xenopus* are conserved, but not interchangeable between zebrafish and *Drosophila*. To test whether this non-overlapping recruitment mechanism is also true for Buc in *Drosophila*, we tested whether ectopic localization of Buc to the anterior pole in *Drosophila* embryos is sufficient to recruit endogenous germ plasm and the subsequent formation of ectopic PGC, as shown for Osk (Ephrussi and Lehmann, 1992). We fused the buc ORF to GFP and a bicoid-3′-UTR to direct its translation to the anterior pole of *Drosophila* embryos (Fig. S3A). As a control, we used sOsk ORF fused to the *bicoid*-3′-UTR (sOsk) (Tanaka and Nakamura, 2008). Immunolabelling of stage 4-5 fly embryos showed that sOsk-GFP can be detected at the anterior pole of the embryos and was sufficient to induce the formation of ectopic PGCs (Fig. S3B,D) by the ectopic localization of germ plasm, including Vasa protein at the anterior pole (Fig. S4). By contrast, although Buc was expressed anteriorly, it was neither anchored to the embryo cortex nor did it ectopically aggregate germ plasm or form ectopic PGCs (Fig. S3E, Fig. S4). These results show that Buc is not recognized by the localization machinery in *Drosophila* that anchors Osk to the cortex and is not sufficient to aggregate germ plasm ectopically, suggesting that zebrafish and flies use different mechanisms for germ plasm recruitment.

The Buc localization signal is part of the conserved N-terminal BUVE motif

To identify the protein domain of Buc that is responsible for its recruitment to the four germ plasm aggregates, we generated systematic deletions of Buc fused to GFP (schematically shown in Fig. 2A), injected their mRNAs into zebrafish one-cell stage zygotes and scored the number of embryos with GFP foci at 3 hpf as depicted in Fig. 1A.

An N-terminal fragment [amino acids (aa) 1-361, Fig. 2A] that corresponds to the previously identified *buc*^{p43} mutant allele localized correctly and with the same penetrance as full-length Buc (Fig. 2A-C, Fig. S5A). Next, we split this fragment into two halves (aa1-158 and 159-361) and analysed their localization. Buc1-158 localized, whereas Buc159-361 showed ubiquitous fluorescence, similar to control embryos injected with GFP mRNA (Fig. 2A,B, Fig. S5B,C). We then split Buc1-158 into two fragments and in addition removed the first ten amino acids (Buc11-88), which show a low conservation in teleost evolution (Škugor et al., 2016). Buc11-88 was sufficient to recapitulate germ plasm localization, whereas Buc89-158 showed no specific localization (Fig. 2A,B,E, Fig. S5D). Further splitting of Buc11-88 disrupted the localization activity of both resulting fragments (Fig. 2A,B, Fig. S5E,F), suggesting that aa11-88 contains the residues sufficient to target the protein to the germ plasm spots. To confirm that Buc does not contain other motifs involved in localization, we generated a deletion of the isolated motif aa11-88 (BucΔ11-88) in full-length Buc. This protein did not localize

Development (2022) 149, dev200465. doi:10.1242/dev.200465

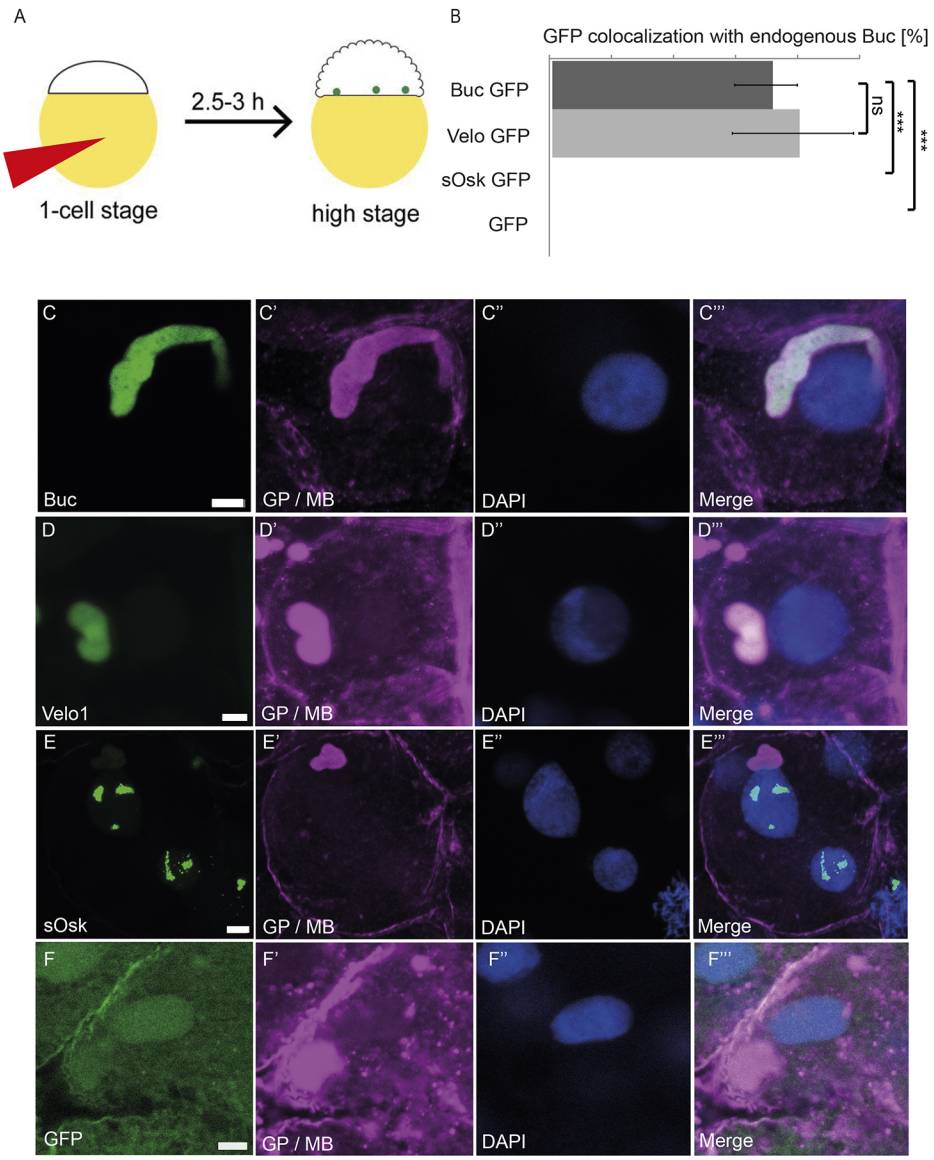

Fig. 1. Buc and Velo1 localize to zebrafish germ plasm. (A) Scheme of zebrafish colocalization assay. RNA encoding GFP fusions of germ plasm organizers Bucky ball (Buc) and Velo1 was injected into one-cell stage embryos and scored at a later stage for localization with endogenous Buc (green dots) by immunohistochemistry. (B) Quantification of colocalization assay. GFP fusions of Buc (71±10.1%) and Velo1 (79.7±19.5%; P=0.6), but not sOsk (0%) or GFP alone (0%), showed colocalization with endogenous Buc. (C-F‴) Magnified germ plasm spot of an embryo at a later stage (full embryos are shown in Fig. S2). Colocalization of GFP (C,D,E,F, green) with endogenous Buc and β-catenin to label membranes (magenta) and nuclei (DAPI, blue) was determined by immunohistochemistry (n=33 for Buc; n=39 for Xvelo; n=32 for GFP). Data are mean±s.d. Scale bars: 5 µm.

(Fig. 2A,B,F). We therefore concluded that aa11-88 is sufficient and necessary for the localization of Buc and named the protein region BucLoc. However, this experiment does not allow us to distinguish whether BucLoc is autonomously anchored at the cleavage furrow or recruited by endogenous Buc in the germ plasm granules. The identified BucLoc domain is part of the so called BUVE domain that shows the highest homology to *Xenopus* Velo1 (Boke et al., 2016; Bontems et al., 2009; Krishnakumar et al., 2018).

Key regions of the Prion-like domains in BucLoc are not required for Buc localization

The BUVE domain was recently shown to be responsible for Velo1 aggregation at the BB during *Xenopus* oogenesis (Boke et al., 2016). The localization of Velo1 to the BB is driven by aggregation of a prion-like domain with two regions enriched in aromatic amino acids within the BUVE motif (Boke et al., 2016). A sequence alignment of Buc with Velo1 showed the conservation of these aromatic amino acids regions of the PLDs in Buc between aa24-30 and 64-71 (Fig. 3A, marked in red), suggesting that these regions might also be required for the formation of the four germ plasm aggregates at the eight-cell stage in zebrafish.

To investigate the importance of these two potential PLD domains in Buc, the colocalization of deletion variants with the germ plasm was analysed. Therefore, mRNA of deletion variants of the BucLoc domain (shown schematically in Fig. 3D) fused to mCherry were injected into one-cell embryos, and their colocalization to germ plasm aggregates marked by Buc-GFP was examined at 3 hpf. As a positive control, we used the entire BucLoc domain (aa11-88) that shows colocalization with the endogenous germ plasm (Fig. 3B,C, quantification in E). To narrow down the localization motif further, the N-terminal 20 amino acids were removed, deleting the N-terminal domain with aromatic amino acids (PLD1; aa21-30). Indeed, Buc 31-88 showed a slight reduction in germ plasm localization (Fig. 3D,E, Fig. S6). However, when we deleted additional ten C-terminal amino acids (Buc31-78), localization was restored to nearly wild-type frequency (Fig. 3D, E, Fig. S7B). By contrast, deleting four additional N-terminal amino acids (Buc35-78) almost completely abrogated localization (Fig. 3D,E). These results suggest that the first PLD does not seem to be necessary for localization.

To examine the role of the second domain with aromatic amino acids (Buc64-71), we generated internal deletions in Buc31-78.

Development (2022) 149, dev200465. doi:10.1242/dev.200465

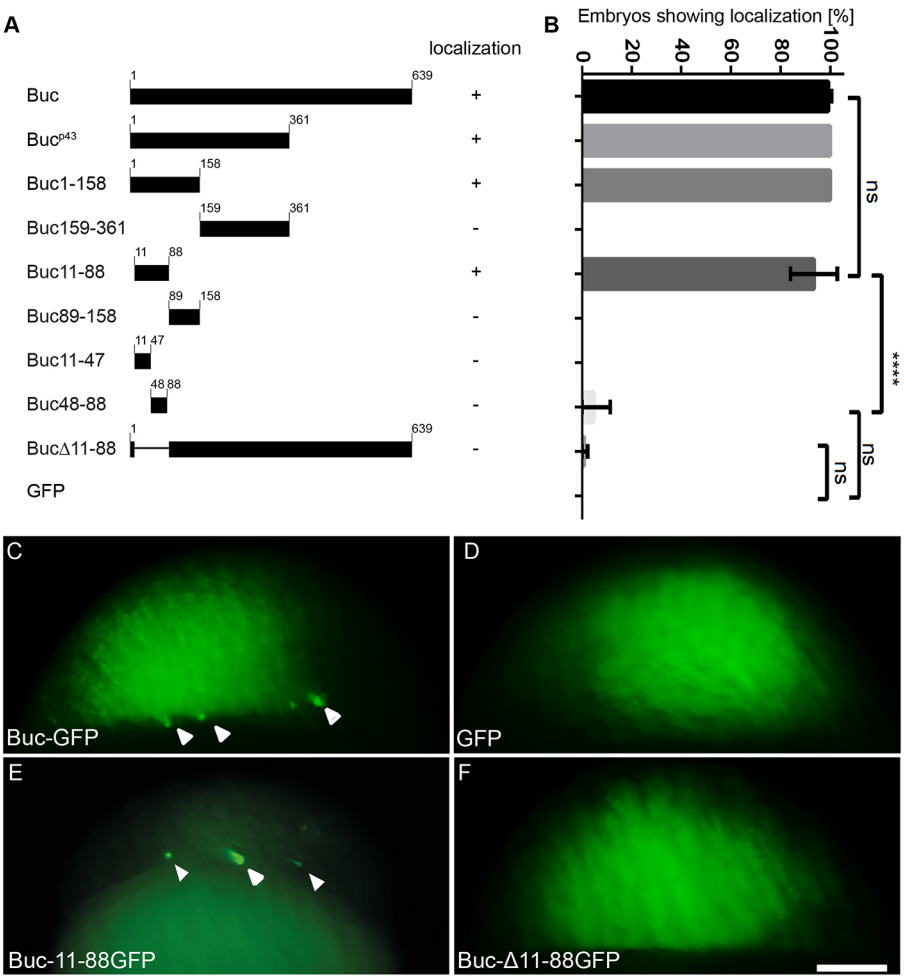

Fig. 2. Buc11-88 is necessary and sufficient for Buc localization in zebrafish embryos. In this localization assay, RNA was injected into one-cell stage embryos and scored at a later stage for localization of fluorescence in living embryos, as shown in Fig. 1A. (A) Schematic representation of Buc protein deletions and a summary of their localization (+/–). Numbers indicate amino acids. (B) Quantification of the localization assay. Buc11-88 localized (90.9±10.1%) similarly to wild-type Buc (99.1±1.3%) (P=0.8). BucΔ11-88 did not localize (0.9±1.6%) compared with wild-type Buc (P=0.009) and Buc11-88 (P=0.01). (C-F) Blastomeres of living later stage embryos oriented as shown in Fig. 1A expressing the indicated constructs. Buc-GFP (C, arrowheads) and Buc11-88 (E, arrowheads) are localized, whereas a GFP-control (D) or BucΔ11-88 (F) show ubiquitous fluorescence (E,G). n=98 for Buc-GFP; n=94 for GFP; n=181 for Buc-11-88GFP; n=230 for Buc-Δ11-88). Data are mean±s.d. Embryos are oriented laterally, with animal pole on top. Scale bar: 100 µm.

When we removed the second PLD (Δ64-71), no fluorescence could be detected in the embryos (Fig. S7C), suggesting that aa64-71 might affect protein stability or translation. Therefore, we analyzed two variants with five amino acid deletions within the second domain. Strikingly, removing parts of the second domain (BucΔ62-66 or BucΔ67-71) caused no clear reduction in germ plasm localization (Fig. 3D,E, Fig. S7D,E). In contrast, when we kept the second domain intact, but removed sequences C-terminal to the second domain (Buc31-71), the localization efficiency dropped to 15% (Fig. 3D,E, Fig. S7F). These results suggest that the two motifs enriched in aromatic amino acids are not required for positioning Buc to the four germ plasm aggregates in the zebrafish embryos.

Identification of the BucLoc interactome

As Buc forms clusters with the germ plasm in the proximity of the cleavage furrows, we aimed to identify the cellular structure that is essential for its anchorage. As our results show that BucLoc domain is sufficient for the recruitment of Buc to the germ plasm foci, we used this protein motif as a bait to identify its cellular binding partners directly by co-immunoprecipitation followed by mass spectrometry analysis. Embryos were injected at the one-cell stage with mRNA encoding BucLoc-GFP, lysed at the stage of the formation of germ plasm foci and immunoprecipitated using GFP-tag (Fig. 4A). Embryos injected with mRNA encoding GFP were used as a negative control, and transgenic embryos for full length Buc-GFP were used to control for mRNA overexpression.

In this analysis, we found 1817 protein candidates that potentially interact with full-length Buc and BucLoc but not with GFP. From those, 213 proteins were strongly enriched for BucLoc interaction (Fig. 4B, see Table S1 for the full list of candidates of the mass spectrometry) and therefore represent candidates for the subcellular network required for germ plasm localization. Among the candidates that were strongly enriched was myosin light chain (Fig. 4C), which is a subunit of the non-muscle myosin II (NMII) protein complex. Interestingly, phosphorylated NMII (p-NMII) colocalizes with germ plasm RNAs at the two- and four-cell stage in zebrafish embryos (Nair et al., 2013). To investigate whether p-NMII also colocalizes with Buc and could therefore play a role in germ plasm localization, we performed immunohistochemistry for Buc and p-NMII. Indeed, we found that Buc colocalizes with p-NMII in early stage IB oocytes (Fig. 4D) and during zebrafish embryogenesis (256 cell stage, Fig. 4E,F). This might suggest a role of NMII in germ plasm localization; however, further experiments might provide a better understanding of this.

As the NMII associates with various cellular structures (Liu et al., 2012; Nair et al., 2013; Vicente-Manzanares et al., 2009), we therefore screened the list of potential BucLoc interactors for a defined subcellular localization. We detected ZO2 and ZF-A89 as highly enriched in the pull-down assay; the latter is a homolog of Cldn-d (UniProtKB/Swiss-Prot record; description: Claudin-like protein ZF-A89) (Table S1). This suggest that we might have purified components of tight junctions. Claudins are adherence

Development (2022) 149, dev200465. doi:10.1242/dev.200465

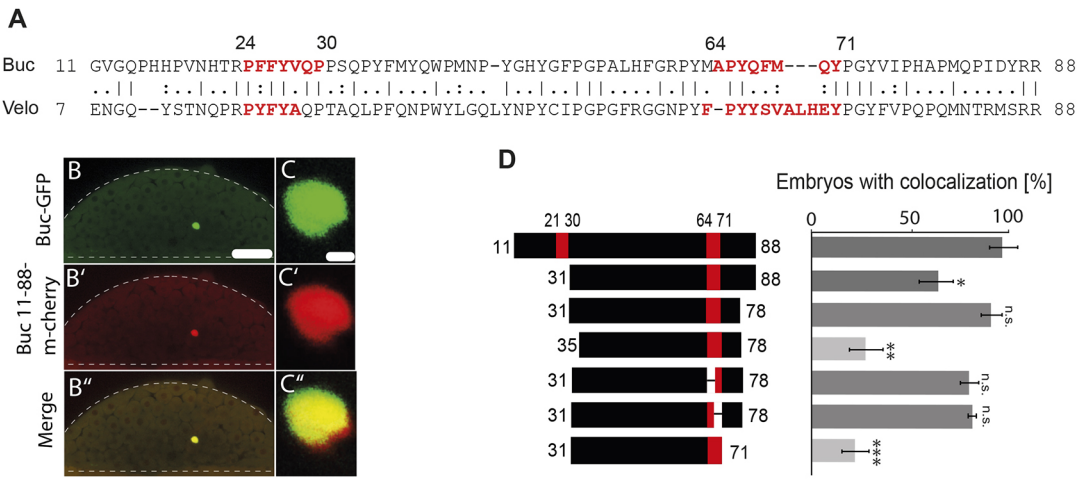

Fig. 3. Localization of BucLoc is not dependent on the aromatic amino acids in the PLD essential for Balbiani Body aggregation. (A) Alignment of Buc11-88 with the N-terminus of *Xenopus* Velo1 (aa7-88). Red letters highlight the regions enriched in aromatic amino acids in the PLD previously discovered in Velo1 (Boke et al., 2016) to be essential for Balbiani Body aggregation and their corresponding amino acids in Buc. (B-C″) BucLoc (11-88)-m-cherry colocalizes to the germ plasm with endogenous Buc-GFP in transgenic embryos. (B-B″) Living sphere stage transgenic Buc-GFP embryo injected at the one-cell stage with RNA encoding BucLoc-m-Cherry, showing colocalization. Embryo is shown in lateral view with the animal pole towards the top, outlined by the white dashed line. (C-C″) Magnification of the localized spot of germ plasm shown in B-B″. (D) Summary of BucLoc mapping showing that the domains enriched in aromatic amino acids (red boxes) are not important for the localization of Buc. PLDs are indicated with red boxes. (E) Quantification of BucLoc mapping and 5aa deletions in D. Buc31-88 (60.1 ±7.9%) and Buc31-71 (21.1±6.4) show significantly less localization compared with Buc11-88 (P=0.01 and 0.0004). There was no significant difference between the localization of Buc11-88 and Buc 31-78 (P=0.41), excluding the role of the first domain enriched in aromatic amino acids in localization. 5aa deletions of Buc31-78 showed that residues other than the second domain with aromatic amino acids are important in the localization of Buc. Buc31-78Δ31-35 (30.0±10) showed significantly less localization compared with Buc31-78 (P=0.009). Colocalization of constructs in D is shown in Fig. S7. n=30 for Buc11-88; n=30 for Buc31-88, Buc31-78, Buc35-78, Buc31-78Δ62-66, Buc31-78Δ67-71 and Buc31-71. Data are mean±s.d. *P≤0.05, **P≤0.01, ***P≤0.001. Scale bars: 50 µm in B; 2 µm in C.

receptors essential for the formation of TJs, suggesting that Buc and germ plasm aggregate at TJs within the cleavage furrows.

Buc colocalizes with tight junction proteins ZO1 and Cldn-d

To further confirm the anchorage of Buc at TJs, we used an antibody that specifically detects the zona occludens protein ZO1, which is shown to directly interact with Cldn proteins to mark the TJ for colocalization analysis. As controls, we used an antibody against E-Cadherin to label the adherens junction and Kif23 to label the midbody. Fascinatingly, Buc perfectly colocalized with the TJ marker ZO1 (Fig. 5D, Fig. S8C), whereas no overlap could be detected with E-Cadherin (Fig. 5B, Fig. S8A) or Kif23 (Fig. 5C, Fig. S8B). These data show that Buc localizes to the ZO1-positive foci at the cleavage furrows, suggesting colocalization of the germ plasm aggregates with TJs. To investigate the localization of Cldn-d, we generated an antibody. Co-labelling of eight-cell embryos with Buc and Cldn-d antibodies showed partial overlapping signals of both proteins (Fig. S9).

By contrast, at germ plasm-free cleavage furrows, we did not detect Buc and Cldn-d colocalization at the membrane. These data support a role of Cldn-d in tethering Buc at the germ plasm cleavage furrows of early zebrafish embryos. However, the absence of Cldn-d protein at those cleavage furrows without germ plasm could also be explained as differences in the temporal development of these furrows.

Taken together, our data show that Buc is associated with Cldn-d and ZO1-positive foci at the cleavage furrows supporting the idea that the TJ protein complex might be functionally involved in the association of Buc and the germ plasm. One limitation of our work is that we cannot show a triple staining of Buc together with Cldn-d and ZO1 due to technical reasons. We therefore suggest further studying the localization of these proteins with regard to other TJs and germ plasm markers.

Electron microscopy showed TJ-like structures at early cleavage furrows

To verify that the ZO1- and Buc-positive structures at the distal cleavage furrows of the eight-cell embryos are TJs, we used electron microscopy to search for characteristic TJ structures at the cleavage furrows of eight-cell stage embryos. Indeed, electron microscopy showed electron-dense membrane sections resembling TJ-like structures at the cleavage furrows where germ plasm is localized (Fig. 5E). In contrast, we did not find these structures at those cleavage furrows, where germ plasm is not accumulated (Fig. 5F). This finding supports the results of staining with the antiserum against ZO1, which also showed four spots in eight-cell stage embryos. The results of the electron microscopy show in addition, for the first time, that early zebrafish embryos already have TJ-like structures at the eight-cell stage. However, we believe the data we provided here are preliminary and limited; we think further electron microscopy is needed to show detailed structure of those embryonic TJs with respect to germ plasm.

The tight junction receptor Cldn-d anchors germ plasm

Claudins are one family of receptors, which physically connect the TJs in the epithelial and endothelial tissues of vertebrates. Claudins are transmembrane proteins that bind to the PDZ domains of scaffolding zonula occludens (ZO) proteins through their cytoplasmic C-terminal YV (tyrosine-valine) motifs (Furuse et al., 2014; McCarthy et al., 2000). More than 50 claudins with restricted tissue expression patterns have been identified in teleost fishes (Kolosov et al., 2013).

The zebrafish genome encodes only five ZO proteins with numerous functions during early zebrafish embryogenesis (Kiener et al., 2007; Schwayer et al., 2019). Fascinatingly, only two claudins, Cldn-d and -e are maternally expressed according to the Zfin database (https://zfin.org/) (Fig. S10). Moreover, the role of the maternally

Development (2022) 149, dev200465. doi:10.1242/dev.200465

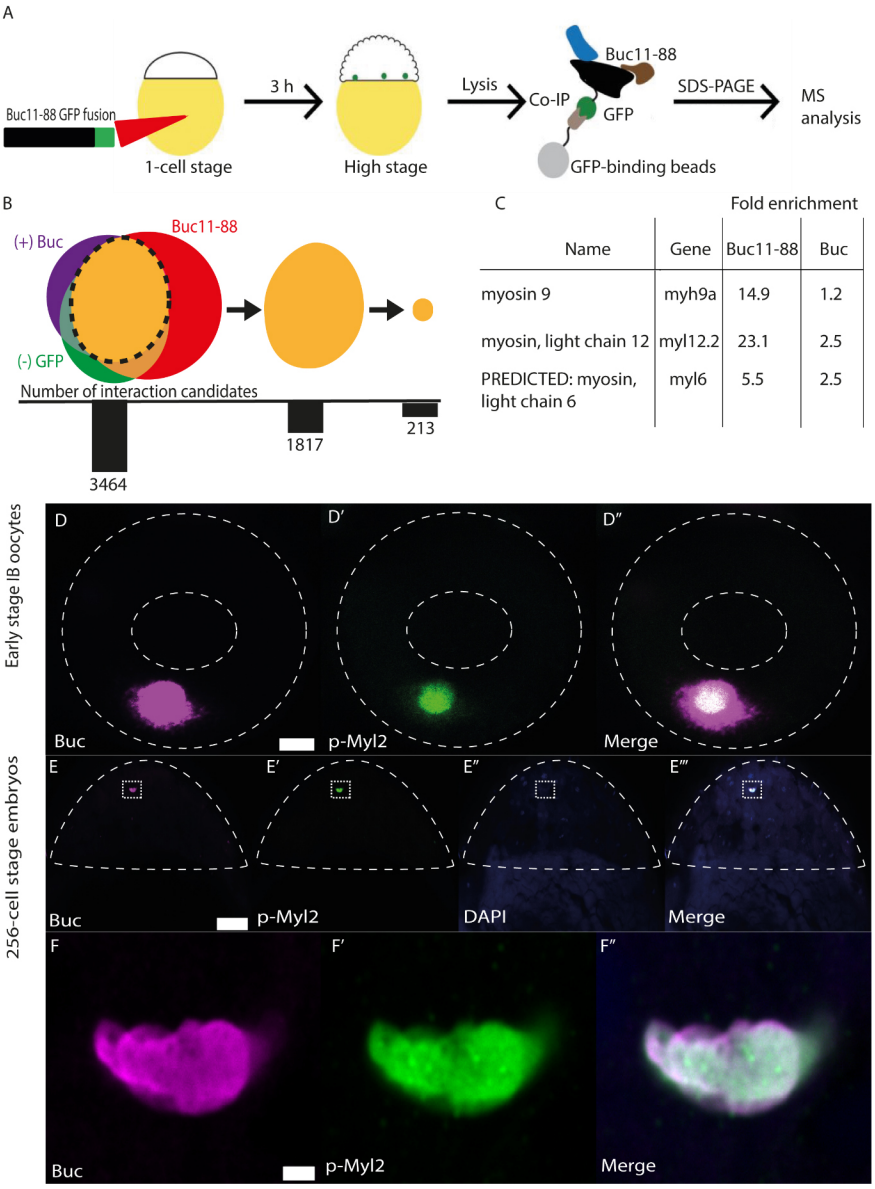

Fig. 4. Non-muscle myosin II (NMII) colocalizes with Buc. Colocalization of Bucky ball (Buc) and phosphorylated myosin light chain 2 (p-Myl2) was determined by immunostaining. (A) Schematic representation of mass spectrometry of BucLoc. Wild-type embryos (*n*=500) were injected with RNA encoding BucLoc-GFP and lysed at a later stage. Embryos of the transgenic Buc-GFP line were used as positive controls. GFP RNA-injected embryos were used as negative controls. After lysis, an immunoprecipitation against the GFP-tag was carried out. Interacting proteins were identified by mass spectrometry. (B) 3464 proteins were identified in the mass spectrometry, of which 1817 candidates interacted with both Buc-GFP and BucLoc-GFP, and 213 interacted specifically with BucLoc-GFP (for selection criteria, see Materials and Methods). (C) Fold enrichment of myosin light chain in the mass spectrometry. (D-D″) Colocalization at an early oocyte stage (immunoblotting). Buc (D, magenta); p-Myl2 (D′, green); merge (D″, white). (E-E‴) Colocalization in an embryo (256 cells). Buc (E, magenta); Myl2 (E′, green); DAPI (E″, blue); merge (E‴, white). (F-F″) Magnification of a germ plasm spot in E,E′,E‴. Scale bars: 10 µm in D-D″; 50 µm in E-E‴; 2 µm in F-F″.

expressed *Xenopus* Xcla, which is an ortholog of Cldn-d, was previously characterized to function in a different process from germ plasm localization, including a dominant-negative version of the receptor (Brizuela et al., 2001). Based on the colocalization of Buc with TJs and the interaction of ZO1 with Cldn-d, we addressed the hypothesis that Cldn-d could act as a membrane anchor for germ plasm.

To analyse a potential function of Cldn-d in germ plasm tethering, we injected *cldn-d* mRNA into one-cell zebrafish embryos transgenic for Buc-GFP to detect germ plasm localization *in vivo*. Compared with uninjected control embryos, the injection of Cldn-d mRNA led to a significantly higher number of Buc-GFP-positive spots at 2-3 hpf (Fig. 6A,B,E). To control the specificity of mRNA overexpression, we injected the same concentration of *cldn-a* mRNA, but did not detect a change of germ plasm spots, similar to uninjected controls (Fig. 6A,C,E).

We believe that our results of control and injected embryos showed no significant difference (Fig. 6G), suggesting that the expression of Cldn-d either caused a fragmentation of the existing four germ plasm spots into more but smaller aggregates or, alternatively, that Cldn-d caused the formation of additional germ plasm aggregates. Independent of the mechanism, these results indicate that Cldn-d might be involved in germ plasm tethering in the early zebrafish embryo. However, further investigation is needed to check the specificity of the function of Cldn-d. It might be worth checking whether Cldn-d overexpression induces ectopic TJ formation versus solely ectopic germ plasm spots, and whether the ectopic spots lead to extra germ cell formation.

The C-terminal amino acids tyrosine and valine are crucial for the interaction of claudins with ZO proteins (Itoh et al., 2014). We therefore generated a Cldn-d mutant lacking this interaction motif (C-terminal YV, named Cldn-dΔYV), which was previously shown to act as a dominant-negative form of claudin-d (Brizuela et al., 2001). Notably, *cldn-dΔYV*-injected embryos showed a significantly reduced number of germ plasm spots in comparison with uninjected embryos (Fig. 6A,D,E). However, *cldn-dΔYV*-injected embryos displayed severe developmental defects, in which the cells did not attach to each other, suggesting that the dominant-negative receptor might also disrupt TJs formed during later embryogenesis (Fig. 6D,D′).

Development (2022) 149, dev200465. doi:10.1242/dev.200465

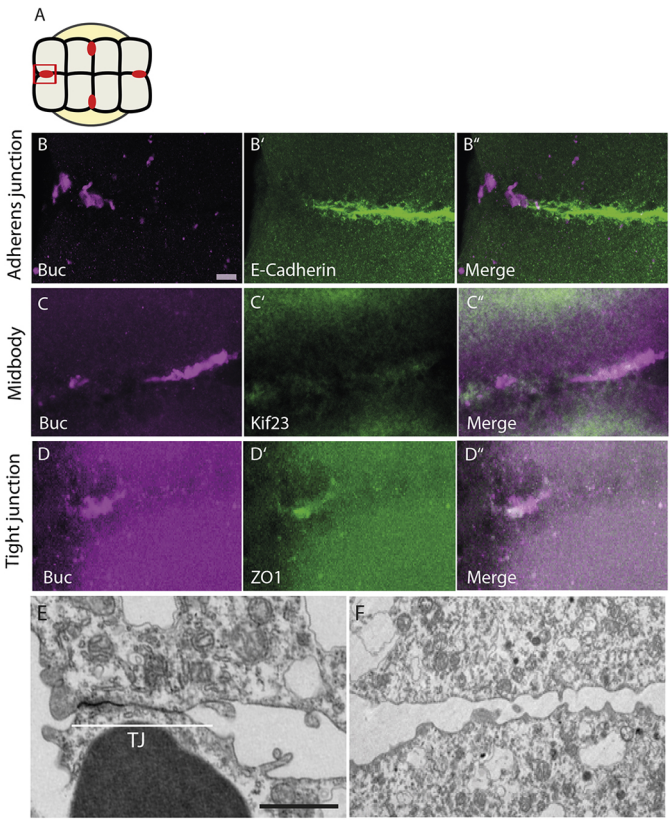

Fig. 5. Buc colocalizes with TJ protein ZO1 and electron microscopy of early cleavage furrows shows TJ-like structures. Colocalization analysis of Buc with different cellular structure markers at the eight-cell stage. (A) A representative cartoon showing an eight-cell stage embryo from the animal view. The red dots show where germ plasm is localized in the cleavage furrows. The cleavage furrows that do not have red dots do not contain germ plasm. The red square represents the cleavage furrows that are shown in the following pictures. (B-D″) Magnification of one of the cleavage furrows containing germ plasm (full embryo staining is shown in Fig. S7). Buc (B,C,D, magenta); respective cellular structure (B′,C′,D′, green); merge (B″,C″,D″). (B-B″) Immunostaining for Buc and the adherens junction marker E-cadherin; (C-C″) Buc and the midbody marker Kif23; (D-D″) Buc and the tight junction marker ZO1. (E) Electron microscopy of germ plasm containing a cleavage furrow. TJ-like structures are observed in this cleavage furrow, as shown with the upper white line, but no germ plasm granules are shown here. (F) Electron microscopy of a non-germ plasm containing cleavage furrow. Scale bars: 5 µm in B-D″; 1 µm in E,F.

To exclude the possibility that the reduced number of germ plasm foci in *cldn-dΔYV*-injected embryos is a secondary result caused by a defect in cell attachment, we targeted its expression to two blastomeres in a 16-cell embryo. Injection of *cldn-dΔYV* mRNA into 16-cell stage embryos still reduces the number of germ plasm spots. At this stage, the junctions are matured and the germ plasm-containing cells can easily be distinguished from somatic cells, as they hold the central position in the marginal row of four blastomeres (‘middle blastomeres’). We injected *cldn-dΔYV* into two middle blastomeres surrounding one germ plasm spot (Fig. 7A) using uninjected and wild-type *cldn-d*-injected embryos as controls. The number of Buc spots was counted immediately after injection (16-cell stage) and then followed up at regular time intervals (see Table S2). In this assay, embryos developed normally and did not show developmental defects (Fig. 7B,C). Interestingly, we still observed a significant reduction in the number of germ plasm spots in *cldn-dΔYV*-injected embryos (Fig. 7B-D) compared with uninjected and *cldn-d*-injected controls (Fig. 7D). More than 35% of *cldn-dΔYV*-injected embryos lost a germ plasm spot, whereas only 6% of the embryos injected with *cldn-d* showed germ plasm spot reduction (Fig. 7D, Table S1). These results support our model that TJs might be involved in the localization of germ plasm at the cleavage furrows and that the Cldn-d receptor might be component of TJs in the early zebrafish embryo (Fig. 8).

DISCUSSION

Our data show that the machinery of germ plasm recruitment and anchorage is different between vertebrates and invertebrates. We identified that the N-terminal BucLoc domain (aa11-88) is necessary and sufficient for the localization of Buc to the four germ plasm aggregates at the cleavage furrow at the eight-cell stage embryo. Our colocalization and protein-protein interaction data from the immunoprecipitations suggest that Buc, together with other germ plasm components, are linked to *de novo*-forming TJs at cleavage furrows.

Our results showed: (1) that myosin light chain co-immunoprecipitated with Buc and that p-NMII colocalizes with Buc protein, suggesting that germ plasm might become anchored to one of the cellular structures through NMII (Fig. 4); (2) co-immunoprecipitations of Buc co-purified ZO and claudin (Fig. 4); (3) that germ plasm colocalizes with the TJ protein ZO1 and with claudin-d (Fig. 5, Figs S8-S10); (4) the presence of TJ-like structures by electron microscopy at the cleavage furrows in the 8-cell zebrafish embryo (Fig. 5); (5) and that *cldn-d* injection caused the formation of a higher number of germ plasm spots, whereas Cldn-d with a mutated interaction motif for ZO proteins (C-terminal YV motif) functions as a potential dominant negative, resulting in fewer germ plasm spots (Figs 6, 7). Taken together, these results might support the model that newly forming TJs at the cleavage furrows represent the anchorage hub for the germ plasm in zebrafish.

Evolutionary conservation of germ plasm anchorage among vertebrates

Invention of multicellularity requires cell adhesion and a more advanced form of reproduction. With our finding, it will be possible to address whether germ plasm localization at TJs was already occurring at the origin of Metazoa or whether it is a derived mechanism acquired during vertebrate evolution. The isolated BucLoc motif does not show homology with known protein domains, making it impossible to trace its biochemical function. However, it suggests a conserved localization mechanism among vertebrates.

Both zebrafish Buc and *Xenopus* xVelo are positioned at the cleavage furrow, whereas *Drosophila* sOsk is not targeted by the vertebrate localization system. Despite the functional equivalence of Buc and Osk shown previously (Krishnakumar et al., 2018), we provide evidence here that the cellular mechanisms of germ plasm anchoring differ between vertebrates and invertebrates. The germ plasm aggregation activity of these germ plasm nucleators appears to be conserved, whereas the mechanisms of their anchoring appear to be different. The observed different mechanisms of germ plasm anchoring are therefore probably consistent with the different morphology of early embryos. Whereas in *Drosophila* the attachment of germ plasm to the apical surface within the syncytial early embryo guarantees the transfer of germ plasm into the budding PGC, we think that in zebrafish the anchoring of germ plasm to the TJs of cleavage furrows is a prerequisite for the asymmetric distribution of germ plasm during subsequent cell divisions; this allows the inheritance of the four germ plasm aggregates into four

Development (2022) 149, dev200465. doi:10.1242/dev.200465

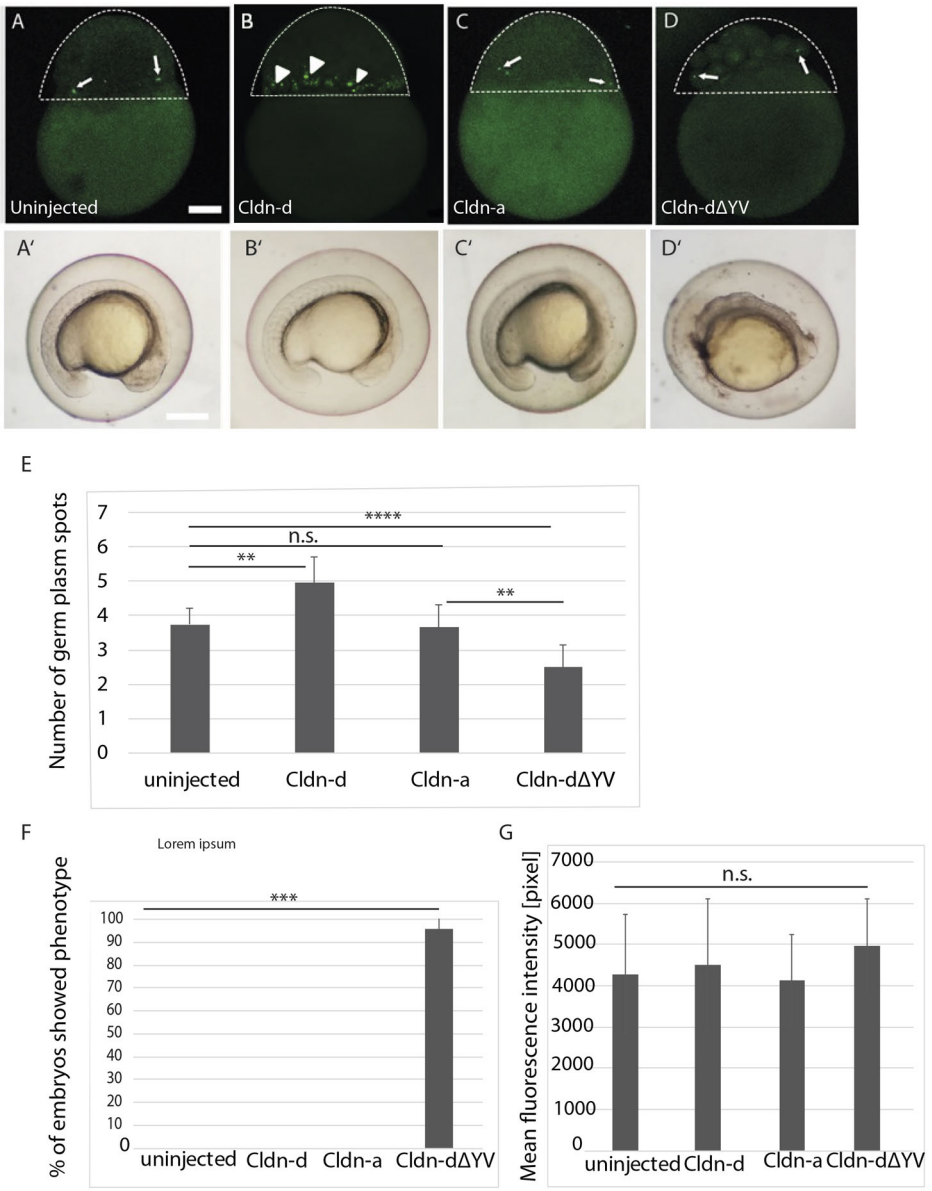

Fig. 6. Cldn-d induces ectopic germ plasm foci. Overexpression of Cldn-d in zebrafish embryos at the one- cell stage. (A) An uninjected embryo from a Buc-GFP transgenic line at 2 hpf. Buc is localized in germ plasm spots. Arrows indicate germ plasm spots. (B) Overexpression of Cldn-d produces additional germ plasm spots (arrowheads). (C) An embryo injected with *cldn-a* show no effect in comparison with control (A). (D) Injection of *cldn-dΔYV* produces a strong phenotype in zebrafish embryos. One embryo is shown here that has developmental defect and its blastomeres are not properly attached to each other. Germ plasm spots are indicated with arrows. (A′-D′) Developed embryos from A-D at 1 dpf (day post fertilization). (A′-D′) Embryos with the head oriented towards the left. (A′) An uninjected embryo, (B′) a *cldn-d* injected embryo, (C′) a *cldn-a* injected embryo and (D′) a *cldn-dΔYV* injected embryo showing developmental defects. (E) Quantification of the average number of germ plasm spots in uninjected and injected embryos. *cldn-a* injection produced no significant difference compared with uninjected control (P=0.3), with average numbers of spots 3.66±0.65 and 3.74±0.48, respectively. *cldn-d* injection caused a significantly higher number of germ plasm spots (4.96±0.76) compared with controls (P=0.004), and *cldn-dΔYV* injection resulted in a significantly lower number of germ plasm spots (2.49 ±0.62) compared with controls (P=0.00003) and *cldn-a* injected embryos (P=0.0049). (F) Quantification of total number of control and injected embryos showing defects in development. Embryos injected with *cldn-dΔYV* showed significant developmental defects compared with uninjected embryos and embryos injected with *cldn-d* and *cldn-a* (P=0.0003). The percentage of *cldn-dΔYV*-injected embryos that showed developmental effect was (95.8±5.89). n=76 for *cldn-d*; n=169 for *cldn-dΔYV*; n=86 for *cldn-a;* n=161 for uninjected. (G) Quantification of total fluorescence in injected and control embryos. No significant difference was recorded between control and *cldn-d*-, *cldn-a*- or *cldn-dΔYV*-injected embryos (P=0.5, 0.8 and 0.7, respectively). n=22 for *cldn-d*; n=24 for *cldn-dΔYV*; n=18 for *cldn-a;* n=21 for uninjected. Data are mean±s.d. **P≤0.01, ***P≤0.001, ****P≤0.0001; n.s., non-significant. Scale bars: 50 µm.

PGCs. However, further experiments disrupting TJs in early embryos might be needed to prove this model.

TJs as an anchorage hub for germ plasm

Anchoring the germ plasm to the TJs is different from anchoring to the posterior cell cortex in *Drosophila* oocytes and embryos long before cellularization take place. In *Drosophila* embryos, the posterior localization of germ plasm is essential for its recruitment into the budding PGCs at the posterior pole. However, in zebrafish embryos, the role of germ plasm anchorage is different. Germ plasm aggregation is detectable from the four-cell stage onwards, and depends on the furrow-associated microtubule-array (FMA)

Development (2022) 149, dev200465. doi:10.1242/dev.200465

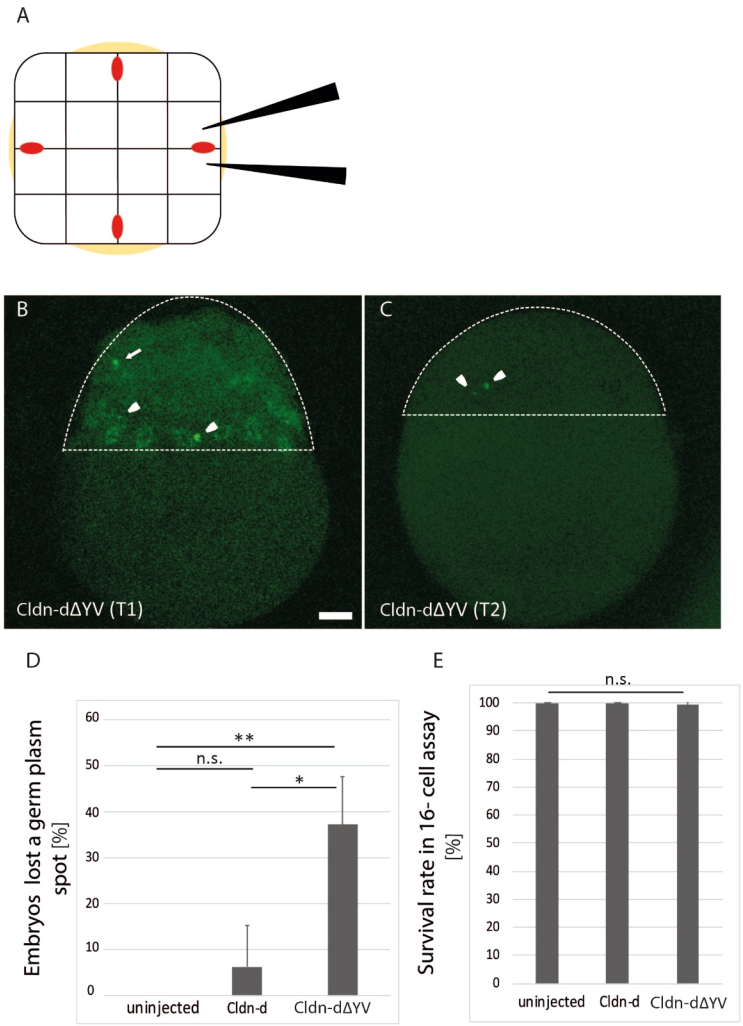

Fig. 7. Cldn-dΔYV reduces the number of germ plasm spots. (A) Schematic representation of a 16-cell injection assay. The embryo is shown in animal view; germ plasm is indicated as red spots. Two middle blastomeres surrounding a single germ plasm spot were injected. (B) A *cldn-dΔYV*-injected embryo from the Buc-GFP transgenic line showing three Buc spots in lateral view (arrow and arrowheads). (C) The same embryo shown in B at 2 hpf. One Buc spot has disappeared (white arrow in B), while the other spots are sustained (arrowheads in B and C). (D) The percentage of embryos that lost a germ plasm spot was significantly higher in *cldn-dΔYV*-injected embryos (35.1±11.2%) than in *cldn-d* injected (6.12±10.8%; P=0.014) or uninjected (0±0.0%; P=0,0024) embryos. No significant difference was seen between Cldn-d-injected and uninjected embryos (P=0.37). (E) Percentage of embryo survival rate in a 16-cell assay. There was no significant difference in the survival rate between injected and control embryos (P=0.43). n=49 for *cldn-d*; n=94 for *cldn-dΔYV*; n=57 for uninjected (see Table S2). Data are mean±s.d. *$P\leq0.05$, **$P\leq0.01$; n.s., non-significant. Scale bar: 50 µm.

(Jesuthasan, 1998; Pelegri et al., 1999) and on the activity of Rho1 and ROCK (Miranda-Rodríguez et al., 2017). However, as the FMA disassembles after the third cleavage, germ plasm needs to be anchored at cleavage furrows. Thus, anchoring to the TJ could represent a functional model that can explain the asymmetric distribution of germ plasm during subsequent cell divisions, with only one of the daughter cells inheriting the TJ and germ plasm at a time. Such an asymmetric distribution of germplasm would explain that starting from the four germ plasm sites at the four-cell stage, only four PGCs arise. It is unclear how germ plasm becomes asymmetrically distributed between the daughter cells and limits the number of aggregates, although several mechanisms are possible:

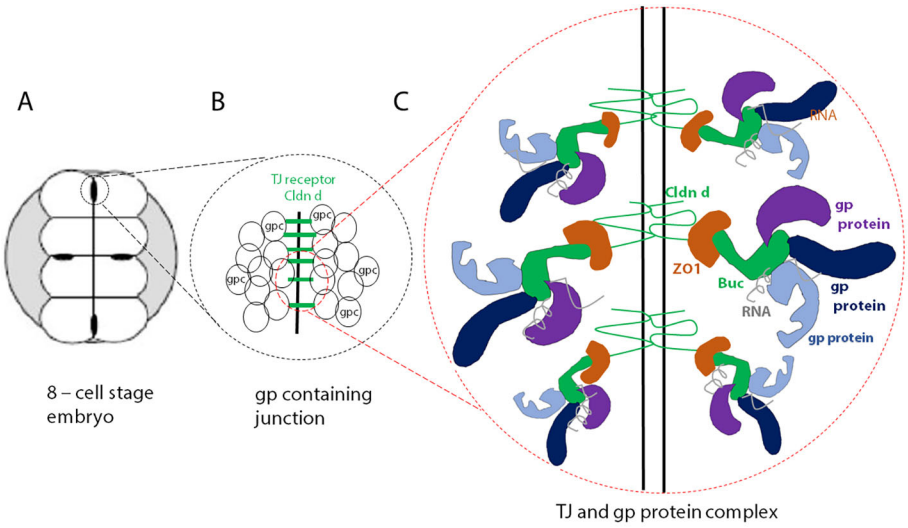

Fig. 8. Proposed model for germ plasm localization in zebrafish. TJs anchor germ plasm at early cleavage furrows in zebrafish embryos. (A) Schematic representation of a zebrafish embryo at the eight-cell stage. Germ plasm is shown in four black spots. (B) Magnification of a germ plasm spot from the embryo in A. Complexes containing germ plasm and TJ proteins (gpc) are anchored to the cleavage furrows by the TJ receptor Cldn-d (green). (C) Representative magnification of the dashed red circle in B. Buc is in a complex with other germ plasm (gp) proteins and RNA interacts with the C-terminal end of Cldn-d. It is currently not known whether Buc binds directly to ZO1.

Development (2022) 149, dev200465. doi:10.1242/dev.200465

(1) removal of the germ granules from the cytoplasmic pool of germ granules during subsequent cleavage divisions; (ii) stabilization of the aggregate and prevention of its fragmentation; and/or (3) facilitation of compaction of the aggregate by phase separation. From the 32-cell stage onwards, germ plasm is associated with a cup-like structure near one spindle pole, which controls asymmetric segregation until the sphere stage (Braat et al., 1999; Knaut et al., 2000; Yoon et al., 1997). Only after the mid-blastula transition (MBT) if germ plasm localized in perinuclear clusters, allowing symmetric distribution during PGC divisions (Strasser et al., 2008) that form four PGC clusters (Kane and Kimmel, 1993; Dosch, 2015; Knaut et al., 2000; Wolke et al., 2002).

We believe that our results show a specific function of Cldn-d for germ plasm anchorage, as injection of Cldn-d caused a significant increase in the number of germ plasm spots, whereas Cldn-a had no effect. The specific role of Cldn-d is supported by the fact that co-immunoprecipitation experiments revealed a specific interaction between Buc and Cldn-d but not with Cldn-a. This differential biological activity suggests a particular capability of Cldn-d to function as a specific anchorage receptor for germ plasm aggregates. Fascinatingly, injection of *cldn-d* had a similar activity on forming extra germ plasm spots compared with the injection of Buc (Bontems et al., 2009). It is unclear yet whether the observed higher number of germ plasm spots represent additional germ plasm spots or a fragmentation of the germ plasm spots already present. Our results suggest that the maternal load of Cldn-d would be limiting and only sufficient to form four spots. Indeed, the loss of spots after injection of dominant-negative Cldn-d seems to support this hypothesis. A specific function of Cldn-d in the anchorage of germ plasm aggregates could explain the release of the germ plasm from TJs by the exchange or dilution of the maternal Cldn-d with other claudins. Alternatively, the release of the germ plasm could be achieved by the post-translational modifications of Buc or components of the TJs.

The recruitment of Buc and *Xenopus* Velo1 to the four germ plasm aggregates in zebrafish suggest also a potential role for Velo1 in germ plasm anchorage in *Xenopus.* A combination of molecular markers, including ZO1, a biotin-based permeability assay and electron microscopy showed that TJs are formed from maternally derived proteins as early as the two-cell stage of *Xenopus* at the boundary between the pre-existing apical membrane and the newly formed basolateral membrane (Fesenko et al., 2000; Merzdorf et al., 1998). Moreover, live imaging studies with Dria-EGFP transgenic *Xenopus* showed that germ plasm aggregates and enters the embryo along cleavage furrows, which are found to be enriched with membranes until embryonic stage 10 after MBT, when germ plasm lose their contact with membranes and become cytoplasmic, presumably associated with perinuclear structures (Taguchi et al., 2012). Based on these similarities it will be valuable to investigate whether the TJ-mediated germ plasm anchoring is also used in *Xenopus* PGCs.

Function of Buc in germ plasm anchorage at the TJs

Sequence analysis of Buc did not reveal any characterized domain within the protein (Bontems et al., 2009; Krishnakumar et al., 2018). Sequence comparison with 15 related Buc proteins revealed a conserved 100 amino acid N-terminus, which was named BUVE motif (Buc-Velo) (Bontems et al., 2009). The BUVE domain was shown to be essential for the formation of the amyloid-like aggregates in the BB in *Xenopus* oocytes (Boke et al., 2016). The BUVE domain contains potential prion like domains (PLDs) (Alberti et al., 2009), which were shown to be essential for the aggregation process, based on the fact that the replacement of critical residues with charged amino acids inhibited the aggregation. These results might suggest that the BUVE domain of Velo1 and Buc is required for amyloid-like germ plasm aggregation in the BB. However, Velo1 variants in which the potential PLDs were replaced with unrelated PLDs were inactive, whereas the replacement with the related sequences from zebrafish Buc were active, revealing a sequence specificity (Boke et al., 2016). Surprisingly intrinsic disorder prediction of Buc showed that the N terminus (aa1-150) is the largest ordered sequence in Buc (Krishnakumar et al., 2018). Nevertheless, we tested for the role of the predicted PLDs within the N-terminus when we identified the region between aa11 and aa88 to be essential and sufficient for the localization of Buc to the four germ plasm spots at the cleavage furrows (Fig. 2). Even though current results cannot rule out the possibility of the exogenous Buc11-88 peptide being incorporated into endogenous Buc protein aggregates, detailed mapping revealed that neither of the two potential PLDs within this sequence is essential for its localization, but short amino acid segments positioned C-terminal from them are essential (Fig. 3). But, this result does not rule out a functional role for the PLDs, as the identified additional regions may be required for proper positioning of the PLDs. However, co-immunoprecipitation and mass spectrometry analyses showed that the domain between aa11 and aa88 interacts with about 213 peptides, including myosin light chain and Cldn-d (Fig. 4), suggesting a role for the BucLoc domain as protein-protein interaction module. However, 213 peptides are an unexpected high number of interactions and includes probably a number of indirect interactions. Future experiments will identify the direct interaction partners of Buc and help to unravel the precise mechanism of Buc anchorage.

Buc and TJs in biomolecular condensates

Increasing evidence suggest that germ granules in many different organisms are formed by phase separation. Germ plasm consists of spherical units of protein RNA aggregates that show a highly dynamic exchange with the surrounding cytoplasm (recently reviewed by Dodson and Kennedy, 2020; So et al., 2021). Indeed, the BucLoc motif has previously been shown to play a crucial role in aggregating the BB in the *Xenopus* oocyte, which is probably the largest biomolecular condensate in the animal kingdom (Boke et al., 2016). However, our results show that the prion-like domains in the BucLoc motif, which control BB assembly, are not required for germ plasm anchoring in the embryo. Moreover, germ plasm aggregates can be detected at the four-cell stage prior to their anchorage to the *de novo* developing TJ, suggesting that germ plasm aggregates are probably formed by phase separation independent of their subsequent anchorage.

Interestingly, ZO proteins also induce the assembly of liquid-like condensates (reviewed by Canever et al., 2020; Citi, 2020). The condensation of ZO proteins in cell culture and zebrafish embryos induces the assembly of TJs, revealing unexpected activity in the cytoplasm to control the formation of TJs (Beutel et al., 2019; Schwayer et al., 2019). Our finding that Buc and ZO1 colocalize raises the issue of whether Buc indeed autonomously induces the formation of condensates or whether this activity is mediated by ZO1. However, we have previously shown Buc condensates in HEK293 cells, which do not form TJs, supporting the autonomous phase separation activity of Buc (Krishnakumar et al., 2018).

Conclusion

In conclusion, we have found that vertebrates and invertebrates use different germ plasm anchorage mechanisms, with evolutionary

Development (2022) 149, dev200465. doi:10.1242/dev.200465

conservation between vertebrates. We have also discovered that TJs anchor germ plasm during early zebrafish embryogenesis and that microinjection of *cldn-d* induced extra germ plasm spots. Therefore, we think that germ plasm in zebrafish is probably anchored to the TJs via Cldn-d receptor protein (Fig. 8).

MATERIALS AND METHODS

Zebrafish handling and manipulation

Zebrafish (*Danio rerio*) used in this study were AB*TLF (wild type) and Buc-GFP transgenic zebrafish lines (Riemer et al., 2015). Fish were raised and maintained according to the guidelines from Westerfield (2000) and according to regulations from the Georg-August University Goettingen.

Microinjection

Previously synthesized capped RNA was diluted with 0.1 M KCl and 0.05% Phenol Red (Sigma Aldrich). 2 nl of RNA was injected into one-cell stage embryos using a PV820 (World Precision Instruments). Injected embryos were incubated in E3 medium at 28°C until they reached the developmental stage of phenotype evaluation.

A 16-cell injection assay of Cldnd-ΔYV

To study whether non-functional Cldn-d has an influence on matured TJs, we conducted *cldn-dΔYV* injections in 16-cell embryos. In this assay, we injected the RNA directly into two cells next to a germ plasm-localizing tight junction. As a control we used uninjected and *cldn-d* RNA-injected embryos. The number of Buc spots was counted immediately after injection and then followed up at regular time periods. The spots were counted from *z*-stacks at ∼2 hpf using an ImageJ plug-in for each *z*-section if the signal-to-background ratio was beyond a specific threshold but with size cut offs to exclude pixel artefacts. A detailed description of the injection procedure at the 16-cell stage has been previously published (Bontems et al., 2009; Krishnakumar et al., 2018).

Drosophila handling and manipulation

Flies were kept and crossed at room temperature or 25°C. To collect embryos, the flies were kept in cages with apple juice agar plates at 25°C. Experiments were approved by the Lower Saxony State Office for Consumer Protection and Food Safety (AZ14/1681). The pUASp *bcd3′* UTR plasmid expressing sOsk (Tanaka and Nakamura, 2008) was used to replace the *sosk* ORF with Buc ORF-GFP. A germline-specific *mat-Gal4VP16* driver was used to express UASp-based transgenes in oogenesis. Antibody staining and fluorescent *in situ* hybridization were performed as described previously (Pflanz et al., 2015). The antibodies used were anti-PY20 (1/500, Biomol; p-Tyrosine, bml-sa240), chicken anti-GFP (1/1000, Synaptic Systems, 132 006), anti-Osk (kindly provided by Anne Ephrussi, European Molecular Biology Laboratory, Heidelberg, Germany) and anti-Vasa (1/5000; Pflanz et al., 2015). Anti-mouse, anti-rabbit and anti-chicken antibodies coupled to Alexa 488, 568 or 647 were used as secondary antibodies (Invitrogen, A-11001, A-11004, A-21235, A-11008, A-11011, A-21244, A-11039, A78950, A78952; 1/1000). Embryos were embedded in DPX to provide clearing and to protect from bleaching.

Biochemical methods

Co-immunoprecipitation

Co-immunoprecipitation (co-IP) was performed to identify the Buc protein interactome. BucLoc interactors were isolated directly from the embryos at the stage where Buc is localized to the putative primordial germ cells to determine the protein network involved in Buc localization. RNA encoding BucLoc-eGFP was introduced into embryos at the one-cell stage, lysed at a higher stage and immunoprecipitated using the GFP tag. As a negative control, embryos injected with RNA encoding eGFP were employed. Embryos from the transgenic Buc-GFP line were used as a positive control for overexpression artefacts. Mass spectrometry was used to analyse the co-immunoprecipitated proteins of the three samples. Each sample was prepared from 500 deyolked high stage embryos after homogenization on ice in lysis buffer [10 mM Tris (pH 7.5), 150 mM NaCl, 0.5 mM EDTA, 0.5% NP-40 and 1× complete protease inhibitor cocktail (Roche)]. The supernatant was subsequently used for the co-IP using a GFP-binding protein coupled to magnetic beads (GFP-Trap_M; ChromoTek) following the manufacturer's instructions. After pulling down, the magnetic beads and their bound proteins were either incubated with 2× SDS loading buffer for 5 min at 96°C and analysed via SDS-PAGE and western blotting or sent for mass spectrometry (Core Facility of Proteome Analysis), as described previously (Krishnakumar et al., 2018).

Selection criteria for specifically interacting proteins

The isolation of the Buc localization domain is a useful approach for determining the mechanism of Buc localization. This tool may be used to investigate which proteins BucLoc interacts with in order to properly locate Buc to the germ plasm during zebrafish development. The molecular network involved in Buc localization is identified, which provides information of the mechanism that underpins the process of localization. In total, 3464 protein candidates interact. From those, 1817 candidates were identified that interacted with both Buc-GFP and BucLoc-GFP. We were not interested in every candidate with an interaction with Buc-GFP, as they might interact with any other region outside BucLoc. Therefore, we applied a set of criteria to identify candidates that significantly interacted with BucLoc. First, any peptide below a background threshold of five in BucLoc-GFP was considered not to be significant and was sorted out. Furthermore, only proteins with counts in BucLoc-GFP that were at least twice as high as in the negative control GFP were considered as significant. To further reduce overexpression artefacts, enrichment in the positive control and in the sample had to be within a magnitude of ±4-fold. Applying these selection criteria, the number of potential BucLoc interaction proteins could be restricted to 213 interaction candidates (see Table S4 for the full list of mass spectrometry candidates).

Immunohistochemistry

Embryos were fixed and stained as previously described (Riemer et al., 2015) with the antibodies listed in Table S5.

Live imaging and image processing

Living embryos of the transgenic Buc-GFP line were imaged to analyse the localization of Buc-GFP. For imaging with the stereo microscope SteREO Lumar.V12 (Zeiss), embryos were manually dechorionated and mounted in 1.5% agarose-coated dishes filled with 1× E3 medium. Images were analysed using the software Axio Vision Rel. 4.8 (Zeiss). For imaging with the LSM780 confocal microscope (Zeiss), embryos were mechanically dechorionated, placed in a fluorodish (World Precision Instruments) with a handmade grid, covered with 1× E3 and imaged from below. Images were analysed using the ZEN 2011 software (Zeiss), as described previously (Riemer et al., 2015). Quantification of confocal images was performed with ImageJ software.

Electron microscopy

Electron microscopy was performed at the facility for transmission electron microscopy (Max Planck Institute for Biophysical Chemistry, Göttingen). Embryos were fixed by high-pressure freezing method and imaged with a Philips CM120 electron microscope using a TemCam 224A slow scan CCD camera, as described previously (Kanagaraj et al., 2016).

Western blotting

Western blotting was performed to detect the specificity of Buc antibody as described previously (Krishnakumar et al., 2018). Fluorescent signal was detected with Li-Cor Odyssey CLx Infrared Imaging system (Li-Cor) and analysed with the Image Studio Software (Li-Cor). Western blots with *in vitro*-translated proteins confirmed that the Buc antibody did not cross-react with GFP or other proteins and thus specifically highlights endogenous germ plasm (Fig. S1). Details of the antibodies used are provided in Table S6.

Development (2022) 149, dev200465. doi:10.1242/dev.200465

In vitro translation

Proteins were synthesized with the TnT SP6 Quick Coupled Transcription/Translation System (Promega).

Molecular biology methods

Cloning

The templates of all the constructs that were used in this study were amplified from reverse-transcribed cDNA, which was made from total ovarian RNA. Constructs were cloned with either restriction digestion or gateway cloning (Table S3).

Bioinformatics

Sequence alignment

Pairwise sequence alignment was used to compare protein sequences, using the Needleman-Wunsch algorithm with the EMBL-EBI alignment software EMBOSS Needle (McWilliam et al., 2013).

PLD prediction

Fold amyloid (Fernandez-Escamilla et al., 2004), APPNN (Família et al., 2015), FISH amyloid (Gasior and Kotulska, 2014) and aggrescan (Conchillo-Solé et al., 2007) algorithms were used to predict PLDs in BucLoc.

Analysis of mass spectrometry data

Overlaps in protein interactions between each co-IP sample were analysed using a Venn diagram generator (http://jura.wi.mit.edu/bioc/tools/venn3way/index.php). The Kyoto Encyclopedia of Genes and Genomes (KEGG, http://www.genome.jp/kegg/) was used to classify the BucLoc-GFP interaction candidates in collaboration with Dr Thomas Lingner to see whether a large number of interaction candidates are involved in the same biochemical pathway. Approximately 62% of the proteins could be assigned to various molecular pathways, including as signalling (11%), splicing (2%), adherens and tight junctions (2%), and mRNA transport, surveillance and destruction (8%). Nevertheless, the co-IP withBucLoc identified 213 interaction candidates involved in various molecular pathways that might play a role in the localization of Buc during early embryogenesis (Table S1).

Statistics

All the statistical analyses of the experiments have been carried out using Microsoft Excel and the Prism software (GraphPad Software). Error bars indicate the standard deviation of averages. For each injection experiment, at least three independent replicates were used.

Acknowledgements

We thank Prof. E. A. Wimmer for providing the facilities to perform this research and G. Kracht for technical assistance. Authors also thank Dr Sabine Klein for the useful input on the manuscript. Data from the PhD theses of Stephan Riemer, Alexander Goloborodko, Nadia Rostam, Roshan Priyarangana Perera and Pritesh Krishnakumar (Georg August University Göttingen, 2014-2020) are presented in this paper.

Competing interests

The authors declare no competing or financial interests.

Author contributions

Conceptualization: R.D.; Methodology: N.R., A.G., S.R., A.H.; Validation: N.R., A.G., S.R.; Formal analysis: N.R., A.G., S.R.; Investigation: N.R., A.G., S.R., A.H., D.R.; Resources: R.D.; Data curation: N.R., A.G., S.R.; Writing - original draft: N.R., G.V., R.D.; Writing - review & editing: N.R., G.V.; Visualization: N.R., A.G., S.R., A.H., D.R.; Supervision: R.D.; Project administration: R.D.; Funding acquisition: R.D.

Funding

This work was supported by a Göttinger Zentrum für Molekulare Biowissenschaften stipend; by a Göttinger Graduiertenzentrum für Neurowissenschaften, Biophysik und Molekulare Biowissenschaften bridging fund (to S.R.); by the Deutscher Akademischer Austauschdienst (to N.R.); by the Deutsche Forschungsgemeinschaft (DO 740/2-3); by a Göttinger Zentrum für Molekulare Biowissenschaften Junior Group stipend; and by the 'Forschungsförderungsprogramm' of the University Medical Center Göttingen (to R.D.). The funders had no role in study design, data collection and analysis, decision to publish or preparation of the manuscript.

References

Aguero, T., Kassmer, S., Alberio, R., Johnson, A. and King, M. L. (2017). Mechanisms of vertebrate germ cell determination. *Adv. Exp. Med. Biol.* **953**, 383-440. doi:10.1007/978-3-319-46095-6

Alberti, S., Halfmann, R., King, O., Kapila, A. and Lindquist, S. (2009). A systematic survey identifies prions and illuminates sequence features of prionogenic proteins. *Cell* **137**, 146-158. doi:10.1016/j.cell.2009.02.044

Beutel, O., Maraspini, R., Pombo-García, K., Martin-Lemaitre, C. and Honigmann, A. (2019). Phase separation of zonula occludens proteins drives formation of tight junctions. *Cell* **179**, 923-936.e11. doi:10.1016/j.cell.2019.10.011

Boke, E., Ruer, M., Wühr, M., Coughlin, M., Lemaitre, R., Gygi, S. P., Alberti, S., Drechsel, D., Hyman, A. A. and Mitchison, T. J. (2016). Amyloid-like self-assembly of a cellular compartment. *Cell* **166**, 637-650. doi:10.1016/j.cell.2016.06.051

Bontems, F., Stein, A., Marlow, F., Lyautey, J., Gupta, T., Mullins, M. C. and Dosch, R. (2009). Bucky ball organizes germ plasm assembly in zebrafish. *Curr. Biol.* **19**, 414-422. doi:10.1016/j.cub.2009.01.038

Braat, A. K., Speksnijder, J. E. and Zivkovic, D. (1999). Germ line development in fishes. *Int. J. Dev. Biol.* **43**, 745-760.

Brizuela, B. J., Wessely, O. and De Robertis, E. M. (2001). Overexpression of the Xenopus tight-junction protein claudin causes randomization of the left-right body axis. *Dev. Biol.* **230**, 217-229. doi:10.1006/dbio.2000.0116

Campbell, P. D., Heim, A. E., Smith, M. Z. and Marlow, F. L. (2015). Kinesin-1 interacts with bucky ball to form germ cells and is required to pattern the zebrafish body axis. *Development (Camb.)* **142**, 2996-3008. doi:10.1242/dev.124586

Canever, H., Sipieter, F. and Borghi, N. (2020). When separation strengthens ties. *Trends Cell Biol.* **30**, 169-170. doi:10.1016/j.tcb.2019.12.002

Citi, S. (2020). Cell biology: tight junctions as biomolecular condensates. *Curr. Biol.* **30**, R83-R86. doi:10.1016/j.cub.2019.11.060

Conchillo-Solé, O., de Groot, N. S., Avilés, F. X., Vendrell, J., Daura, X. and Ventura, S. (2007). AGGRESCAN: a server for the prediction and evaluation of "hot spots" of aggregation in polypeptides. *BMC Bioinformatics* **8**, 65. doi:10.1186/1471-2105-8-65

Dodson, A. E. and Kennedy, S. (2020). Phase separation in germ cells and development. *Dev. Cell* **55**, 4-17. doi:10.1016/j.devcel.2020.09.004

Dosch, R. (2015). Next generation mothers: maternal control of germline development in zebrafish. *Crit. Rev. Biochem. Mol. Biol.* **50**, 54-68. doi:10.3109/10409238.2014.985816

Ephrussi, A. and Lehmann, R. (1992). Induction of germ cell formation by oskar. *Nature* **358**, 387-392. doi:10.1038/358387a0

Ewen-Campen, B., Schwager, E. E. and Extavour, C. G. M. (2010). The molecular machinery of germ line specification. *Mol. Reprod. Dev.* **77**, 3-18. doi:10.1002/mrd.21091

Família, C., Dennison, S. R., Quintas, A. and Phoenix, D. A. (2015). Prediction of peptide and protein propensity for amyloid formation. *PLoS ONE* **10**, 1-16. doi:10.1371/journal.pone.0134679

Fernandez-Escamilla, A.-M., Rousseau, F., Schymkowitz, J. and Serrano, L. (2004). Prediction of sequence-dependent and mutational effects on the aggregation of peptides and proteins. *Nat. Biotechnol.* **22**, 1302-1306. doi:10.1038/nbt1012

Fesenko, I., Kurth, T., Sheth, B., Fleming, T. P., Citi, S. and Hausen, P. (2000). Tight junction biogenesis in the early Xenopus embryo. *Mech. Dev.* **96**, 51-65. doi:10.1016/S0925-4773(00)00368-3

Furuse, M., Fujita, K., Hiiragi, T., Fujimoto, K. and Tsukita, S. (2014). Claudin-1 and -2: novel integral membrane proteins localizing at tight junctions with no sequence similarity to occludin. *J. Cell Biol.* **141**, 1539-1550. doi:10.1083/jcb.141.7.1539

Gasior, P. and Kotulska, M. (2014). FISH Amyloid - a new method for finding amyloidogenic segments in proteins based on site specific co-occurence of aminoacids. *BMC Bioinformatics* **15**, 1-8. doi:10.1186/1471-2105-15-54

Heasman, J., Quarmby, J. and Wylie, C. C. (1984). The mitochondrial cloud of Xenopus oocytes: the source of germinal granule material. *Dev. Biol.* **105**, 458-469. doi:10.1016/0012-1606(84)90303-8

Heim, A. E., Hartung, O., Rothhämel, S., Ferreira, E., Jenny, A. and Marlow, F. L. (2014). Oocyte polarity requires a Bucky ball-dependent feedback amplification loop. *Development (Camb.)* **141**, 842-854. doi:10.1242/dev.090449

Houston, D. W. (2013). Regulation of cell polarity and RNA localization in vertebrate oocytes. In *International Review of Cell and Molecular Biology* *ed. K. W. Jeon), pp. 127-185. Elsevier. doi:10.1016/B978-0-12-407694-5.00004-3

Houwing, S., Kamminga, L. M., Berezikov, E., Cronembold, D., Girard, A., van den Elst, H., Filippov, D. V., Blaser, H., Raz, E., Moens, C. B. et al. (2007). A role for Piwi and piRNAs in germ cell maintenance and transposon silencing in zebrafish. *Cell* **129**, 69-82. doi:10.1016/j.cell.2007.03.026

Itoh, M., Furuse, M. and Morita, K. (2014). Direct binding of three tight junction-associated and ZO-3, with the COOH termini of claudins. *J. Cell Biol.* **147**, 1351-1363. doi:10.1083/jcb.147.6.1351

Jeske, M., Müller, C. W. and Ephrussi, A. (2017). The LOTUS domain is a conserved DEAD-box RNA helicase regulator essential for the recruitment of Vasa to the germ plasm and nuage. *Genes Dev.* **31**, 939-952. doi:10.1101/gad.297051.117

Jesuthasan, S. (1998). Furrow-associated microtubule arrays are required for the cohesion of zebrafish blastomeres following cytokinesis. *J. Cell Sci.* **111**, 3695-3703. doi:10.1242/jcs.111.24.3695
Juliano, C. E., Swartz, S. Z. and Wessel, G. M. (2010). A conserved germline multipotency program. *Development* **137**, 4113-4126. doi:10.1242/dev.047969
Kanagaraj, P., Riedel, D. and Dosch, R. (2016). High-pressure freezing electron microscopy of zebrafish oocytes. *Methods Mol. Biol.* **1457**, 167-178. doi:10.1007/978-1-4939-3795-0_12.
Kane, D. A. and Kimmel, C. B. (1993). The zebrafish midblastula transition. *Development* **119**, 447-456. doi:10.1242/dev.119.2.447
Kiener, T. K., Sleptsova-Friedrich, I. and Hunziker, W. (2007). Identification, tissue distribution and developmental expression of tjp1/zo-1, tjp2/zo-2 and tjp3/zo-3 in the zebrafish, Danio rerio. *Gene Expr. Patterns* **7**, 767-776. doi:10.1016/j.modgep.2007.05.006
Kim-Ha, J., Webster, P. J., Smith, J. L. and Macdonald, P. M. (1993). Multiple RNA regulatory elements mediate distinct steps in localization of oskar mRNA. *Development* **119**, 169-178. doi:10.1242/dev.119.1.169
Kistler, K. E., Trcek, T., Hurd, T. R., Chen, R., Liang, F.-X., Sall, J., Kato, M. and Lehmann, R. (2018). Phase transitioned nuclear oskar promotes cell division of drosophila primordial germ cells. *eLife* **7**, 1-35. doi:10.7554/eLife.37949
Knaut, H., Pelegri, F., Bohmann, K., Schwarz, H. and Nüsslein-Volhard, C. (2000). Zebrafish vasa RNA but not its protein is a component of the germ plasm and segregates asymmetrically before germline specification. *J. Cell Biol.* **149**, 875-888. doi:10.1083/jcb.149.4.875
Kolosov, D., Bui, P., Chasiotis, H. and Kelly, S. P. (2013). Claudins in teleost fishes. *Tissue Barriers* **1**, e25391. doi:10.4161/tisb.25391
Krishnakumar, P., Riemer, S., Perera, R., Lingner, T., Goloborodko, A., Khalifa, H., Bontems, F., Kaufholz, F., El-Brolosy, M. A. and Dosch, R. (2018). Functional equivalence of germ plasm organizers. *PLoS Genet.* **14**, 1-29. doi:10.1371/journal.pgen.1007696
Liu, K. C., Jacobs, D. T., Dunn, B. D., Fanning, A. S. and Cheney, R. E. (2012). Myosin-X functions in polarized epithelial cells. *Mol. Biol. Cell* **23**, 1675-1687. doi:10.1091/mbc.e11-04-0358
Marlow, F. L. and Mullins, M. C. (2008). Bucky ball functions in Balbiani body assembly and animal-vegetal polarity in the oocyte and follicle cell layer in zebrafish. *Dev. Biol.* **321**, 40-50. doi:10.1016/j.ydbio.2008.05.557
McCarthy, K. M., Francis, S. A., McCormack, J. M., Lai, J., Rogers, R. A., Skare, I. B., Lynch, R. D. and Schneeberger, E. E. (2000). Inducible expression of claudin-1-myc but not occludin-VSV-G results in aberrant tight junction strand formation in MDCK cells. *J. Cell Sci.* **3398**, 3387-3398. doi:10.1242/jcs.113.19.3387
McWilliam, H., Li, W., Uludag, M., Squizzato, S., Park, Y. M., Buso, N., Cowley, A. P. and Lopez, R. (2013). Analysis Tool Web Services from the EMBL-EBI. *Nucleic Acids Res.* **41**, 597-600. doi:10.1093/nar/gkt376
Merzdorf, C. S., Chen, Y.-H. and Goodenough, D. A. (1998). Formation of functional tight junctions in Xenopus embryos. *Dev. Biol.* **195**, 187-203. doi:10.1006/dbio.1997.8846
Miranda-Rodríguez, J. R., Salas-Vidal, E., Lomelí, H., Zurita, M. and Schnabel, D. (2017). RhoA/ROCK pathway activity is essential for the correct localization of the germ plasm mRNAs in zebrafish embryos. *Dev. Biol.* **421**, 27-42. doi:10.1016/j.ydbio.2016.11.002
Moravec, C. E. and Pelegri, F. (2020). The role of the cytoskeleton in germ plasm aggregation and compaction in the zebrafish embryo. *Curr. Top. Dev. Biol.* **140**, 145-179. doi:10.1016/bs.ctdb.2020.02.001.
Nair, S., Marlow, F., Abrams, E., Kapp, L., Mullins, M. C. and Pelegri, F. (2013). The chromosomal passenger protein birc5b organizes microfilaments and germ plasm in the zebrafish embryo. *PLoS Genet.* **9**, e1003448. doi:10.1371/journal.pgen.1003448
Olsen, L. C., Aasland, R. and Fjose, A. (1997). A vasa-like gene in zebrafish identifies putative primordial germ cells. *Mech. Dev.* **66**, 95-105. doi:10.1016/S0925-4773(97)00099-3
Otto, S. P. and Goldstein, D. B. (1992). Recombination and the evolution of diploidy. *Genetics* **131**, 745-751. doi:10.1093/genetics/131.3.745
Pelegri, F., Knaut, H., Maischein, H.-M., Schulte-Merker, S. and Nüsslein-Volhard, C. (1999). A mutation in the zebrafish maternal-effect gene nebel affects furrow formation and vasa RNA localization. *Curr. Biol.* **9**, 1431-1440. doi:10.1016/S0960-9822(00)80112-8
Pflanz, R., Voigt, A., Yakulov, T. and Jäckle, H. (2015). Drosophila gene tao-1 encodes proteins with and without a Ste20 kinase domain that affect cytoskeletal architecture and cell migration differently. *Open Biol.* **5**, 140161. doi:10.1098/rsob.140161
Raz, E. (2003). Primordial germ-cell development: The zebrafish perspective. *Nat. Rev. Genet.* **4**, 690-700. doi:10.1038/nrg1154
Ressom, R. E. and Dixon, K. E. (1988). Relocation and reorganization of germ plasm in Xenopus embryos after fertilization. *Development* **103**, 507-518. doi:10.1242/dev.103.3.507
Riemer, S., Bontems, F., Krishnakumar, P., Gömann, J. and Dosch, R. (2015). A functional Bucky ball-GFP transgene visualizes germ plasm in living zebrafish. *Gene Expr. Patterns* **18**, 44-52. doi:10.1016/j.gep.2015.05.003
Roovers, E. F., Kaaij, L. J. T., Redl, S., Bronkhorst, A. W., Wiebrands, K., de Jesus Domingues, A. M., Huang, H.-Y., Han, C.-T., Riemer, S., Dosch, R. et al. (2018). Tdrd6a regulates the aggregation of buc into functional subcellular compartments that drive germ cell specification. *Dev. Cell* **46**, 285-301.e9. doi:10.1016/j.devcel.2018.07.009
Schwayer, C., Shamipour, S., Pranjic-Ferscha, K., Schauer, A., Balda, M., Tada, M., Matter, K. and Heisenberg, C.-P. (2019). Mechanosensation of tight junctions depends on ZO-1 phase separation and flow. *Cell* **179**, 937-952.e18. doi:10.1016/j.cell.2019.10.006
Seydoux, G. (2018). The P granules of C. elegans: a genetic model for the study of RNA–protein condensates. *J. Mol. Biol.* **430**, 4702-4710. doi:10.1016/j.jmb.2018.08.007
Škugor, A., Tveiten, H., Johnsen, H. and Andersen, Ø. (2016). Multiplicity of Buc copies in Atlantic salmon contrasts with loss of the germ cell determinant in primates, rodents and axolotl. *BMC Evol. Biol.* **16**, 232. doi:10.1186/s12862-016-0809-7
So, C., Cheng, S. and Schuh, M. (2021). Phase separation during germline development. *Trends Cell Biol.* **31**, 254-268. doi:10.1016/j.tcb.2020.12.004
Strasser, M. J., Mackenzie, N. C., Dumstrei, K., Nakkrasae, L.-I., Stebler, J. and Raz, E. (2008). Control over the morphology and segregation of Zebrafish germ cell granules during embryonic development. *BMC Dev. Biol.* **8**, 58. doi:10.1186/1471-213X-8-58
Strome, S. and Updike, D. (2015). Specifying and protecting germ cell fate. *Nat. Rev. Mol. Cell Biol.* **16**, 406-416. doi:10.1038/nrm4009
Strome, S. and Wood, W. B. (1983). Generation of asymmetry and segregation of germ-line granules in early C. elegans embryos. *Cell* **35**, 15-25. doi:10.1016/0092-8674(83)90203-9
Taguchi, A., Tak, M., Motoishi, M., Or, H., Moch, M. and Watanabe, K. (2012). Analysis of localization and reorganization of germ plasm in Xenopus transgenic line with fluorescence-labeled mitochondria. *Dev. Growth Differ.* **54**, 767-776. doi:10.1111/dgd.12005
Tanaka, T. and Nakamura, A. (2008). The endocytic pathway acts downstream of Oskar in Drosophila germ plasm assembly. *Development* **135**, 1107-1117. doi:10.1242/dev.017293
Trcek, T. and Lehmann, R. (2019). Germ granules in Drosophila. *Traffic* **20**, 650-660. doi:10.1111/tra.12674
Vicente-Manzanares, M., Ma, X., Adelstein, R. S. and Horwitz, A. R. (2009). Non-muscle myosin II takes centre stage in cell adhesion and migration. *Nat. Rev. Mol. Cell Biol.* **10**, 778-790. doi:10.1038/nrm2786
Welch, E. and Pelegri, F. (2014). Cortical depth and differential transport of vegetally localized dorsal and germ line determinants in the zebrafish embryo. *BioArchitecture* **5**, 13-26. doi:10.1080/19490992.2015.1080891
Westerfield, M. (2000). *No TitleThe Zebrafish book: A Guide for the Laboratory Use of Zebrafish(Danio rerio)*, 4th edn. Eugene: University of Oregon Press.
Wolke, U., Weidinger, G., Köprunner, M. and Raz, E. (2002). Multiple levels of posttranscriptional control lead to germ line-specific gene expression in the zebrafish. *Curr. Biol.* **12**, 289-294. doi:10.1016/S0960-9822(02)00679-6
Yabe, T., Ge, X. and Pelegri, F. (2007). The zebrafish maternal-effect gene cellular atoll encodes the centriolar component sas-6 and defects in its paternal function promote whole genome duplication. *Dev. Biol.* **312**, 44-60. doi:10.1016/j.ydbio.2007.08.054
Yoon, C., Kawakami, K. and Hopkins, N. (1997). Zebrafish vasa homologue RNA is localized to the cleavage planes of 2- and 4-cell-stage embryos and is expressed in the primordial germ cells. *Development* **124**, 3157-3165. doi:10.1242/dev.124.16.3157

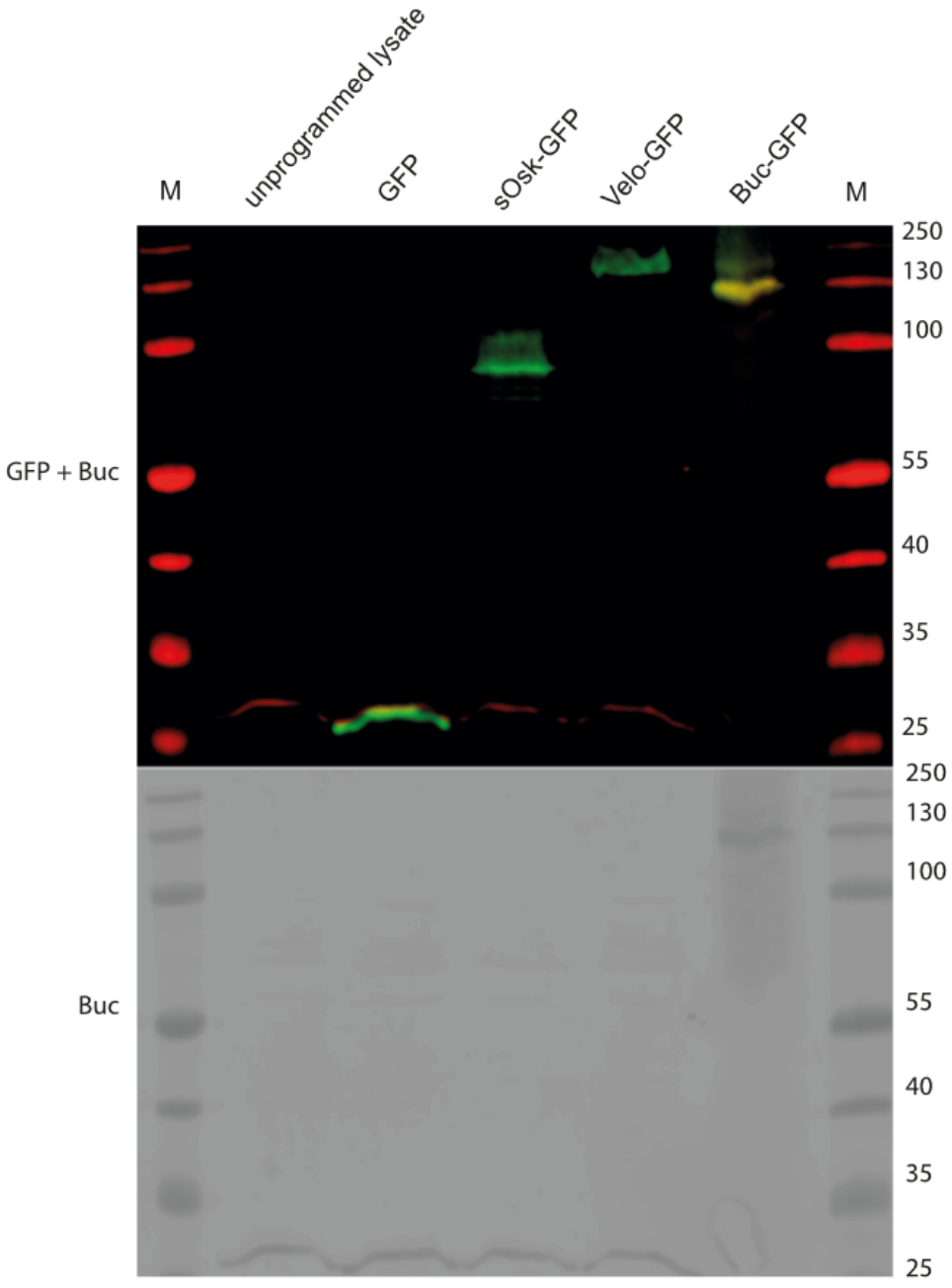

Fig. S1. The Buc antibody does not cross-react with GFP, *Xenopus* Velo or *Drosophila* Oskar. Western blot showing anti-Buc (red in upper panel and black in lower panel) or anti-GFP (green in upper panel) antibody staining of *in vitro* translated GFP, sOsk-GFP, Velo-GFP and Buc-GFP. Unprogrammed lysate was used as negative control for protein translation. Buc-GFP is visualized by both anti-Buc and anti-GFP antibodies (yellow in merged panel and black in lower panel), whereas Velo-GFP, sOsk-GFP and GFP are only recognized by anti-GFP antibody, but not by anti-Buc antibody.

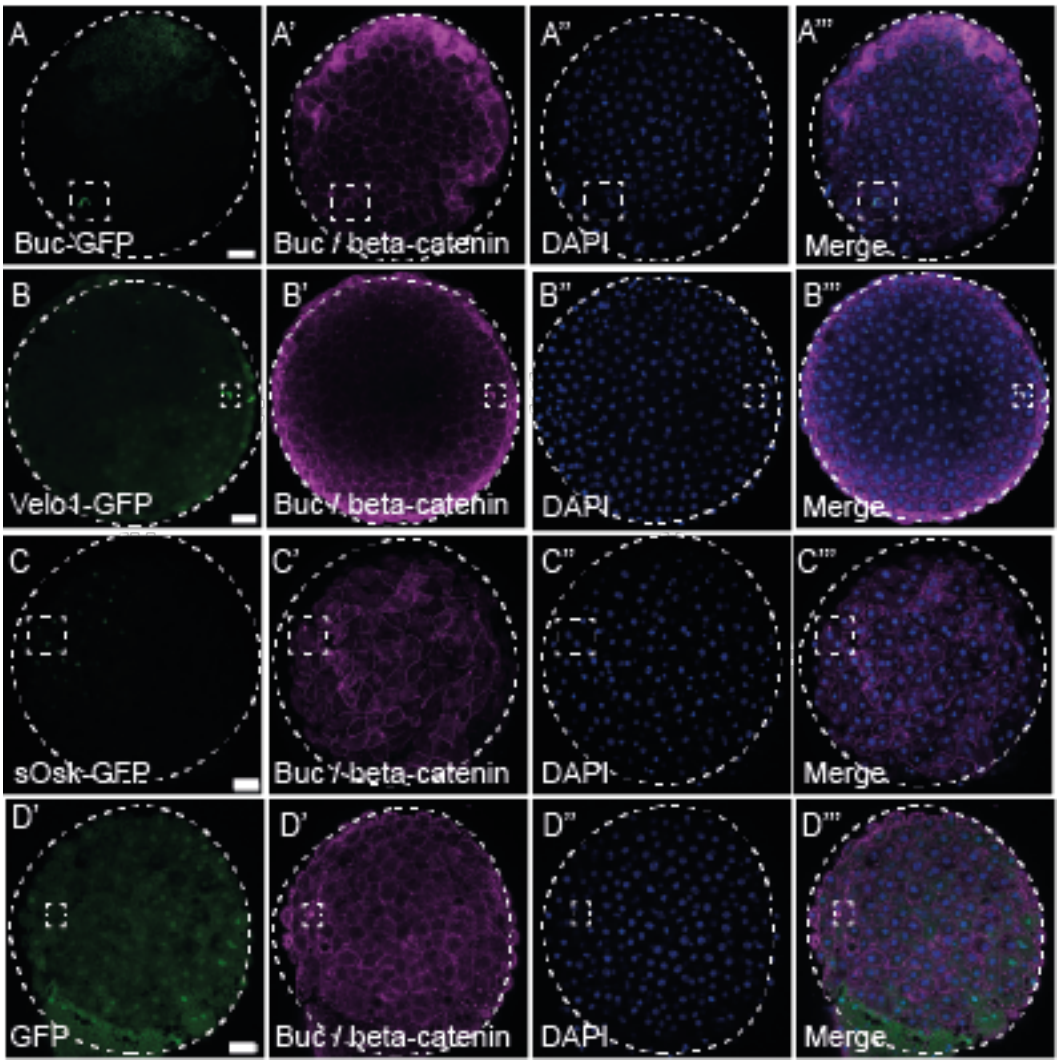

Fig. S2. Germ plasm localization is conserved in vertebrates.

Panels (A,B,C,D) show embryos at high stage from the animal view. Dotted circles outline the embryos. Dotted rectangles show magnified areas in figure 1. Colocalization of the GFP with endogenous Buc was determined by immunohistochemistry: 1st column – injected GFP fusions (green), 2nd column – endogenous Buc and beta-catenin (magenta), 3rd column – DAPI (blue) and 4th column – merge. Buc-GFP (A-A''') and *Xenopus* Velo1 (B-B''') colocalize with endogenous germ plasm, whereas *Drosophila* Osk(C-C''') shows nuclear localization. The GFP control shows ubiquitous low level fluorescence (D-D'''). Scalebars: 50 µm.

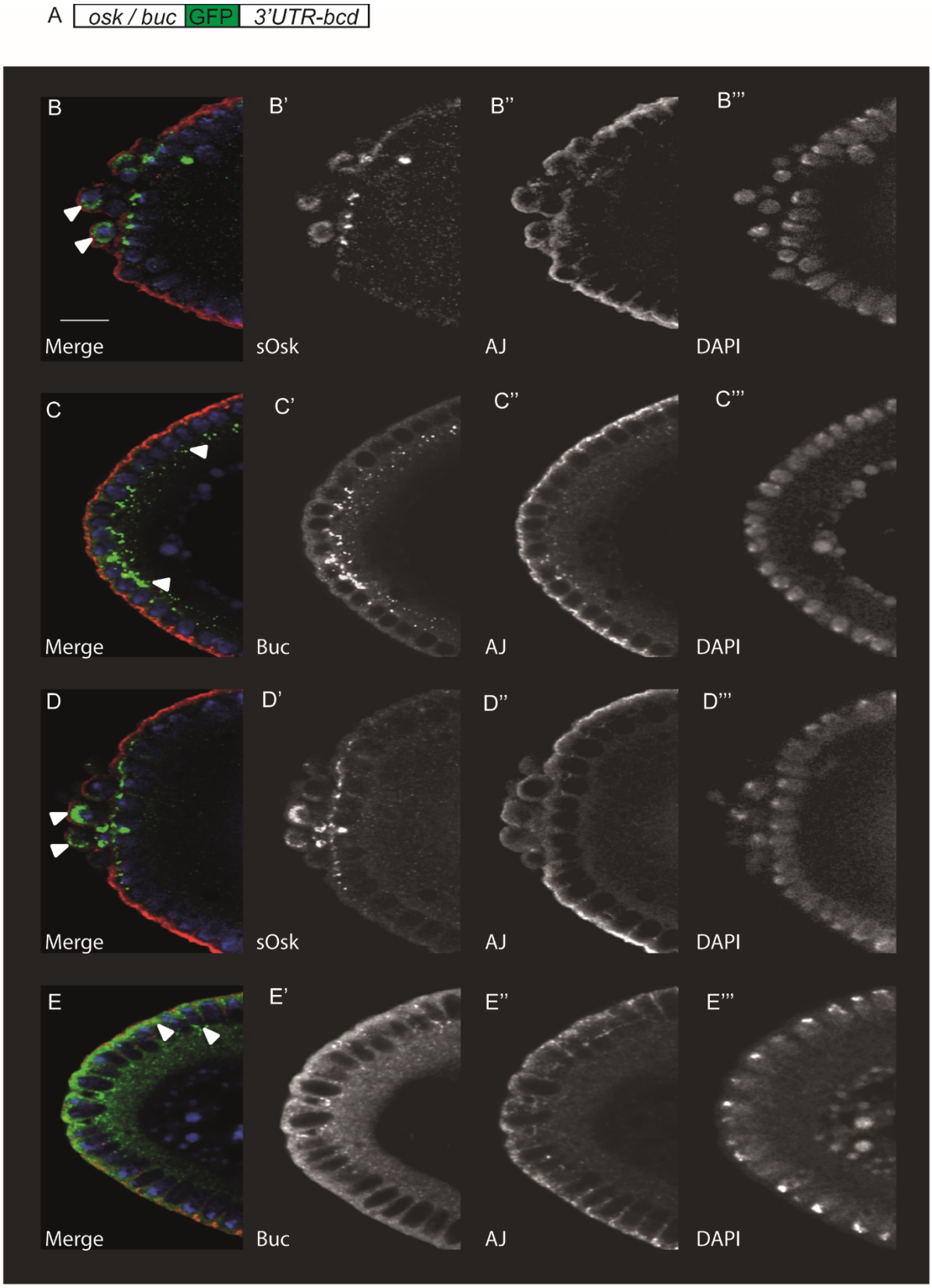

Fig. S3. Transgenic Buc- and Oskar-GFP *Drosophila* embryos show different localization patterns.

(A) Scheme of transgenes to study Bucky ball (Buc) and short Oskar (sOsk) localization. Transgenic flies were generated expressing Buc-GFP or sOsk ectopically at the anterior pole of the embryo by fusion of the constructs to the *bicoid* 3'UTR. (B-E) Localization of sOsk and Buc-GFP was investigated by immunohistochemistry: 1st column – merge, 2nd column – expressed protein, 3rd column – apical junctions (AJ), 4th column – DAPI. Anterior pole of immunostained embryos expressing the indicated transgenic constructs at stage 4 (B, C) and 5 (D, E). sOsk (B, B', D, D') localizes in condensed aggregates at the most distal part of the anterior pole (white arrowheads), whereas Buc-GFP (C, C', E, E') distributes in a gradient along the cortex of the anterior pole (white arrowheads). Scale bar: 10 µm.

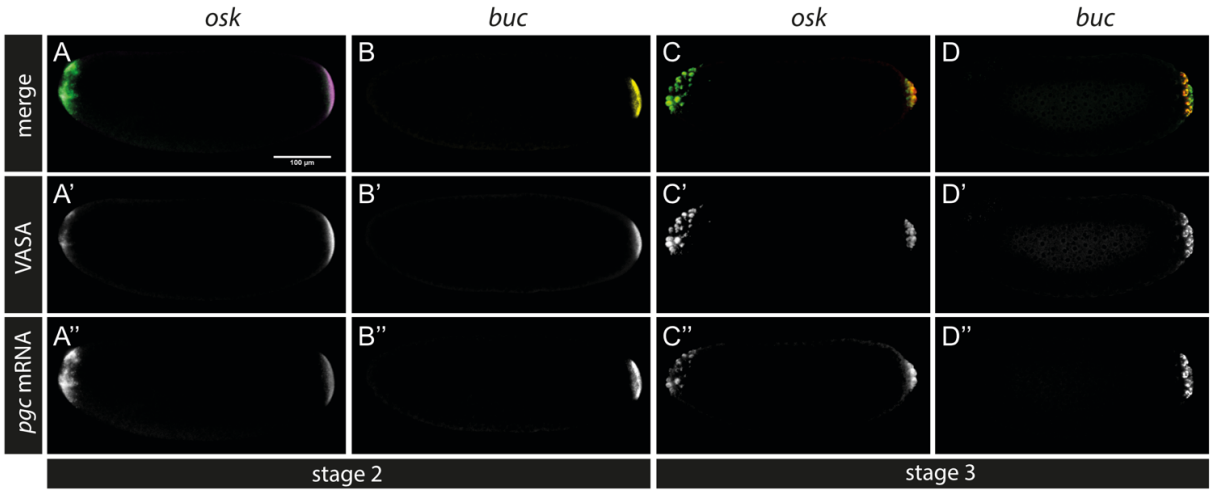

Fig. S4. Vasa protein and pgc mRNA recruitment in transgenic flies.

Vasa protein and *pgc* mRNA labeling of the transgenic embryos showed that sOsk specified ectopic PGCs, whereas Buc transgenics did not recruit Vasa protein or *pgc* mRNA at the anterior pole. (A-A'', B-B'') show VASA and *pgc* labeling of sOsk and Buc in stage2 transgenic flies. (C-C'', D-D'') show VASA and *pgc* labeling of sOsk and Buc in stage3 transgenic flies. Scale bar: 100 µm.

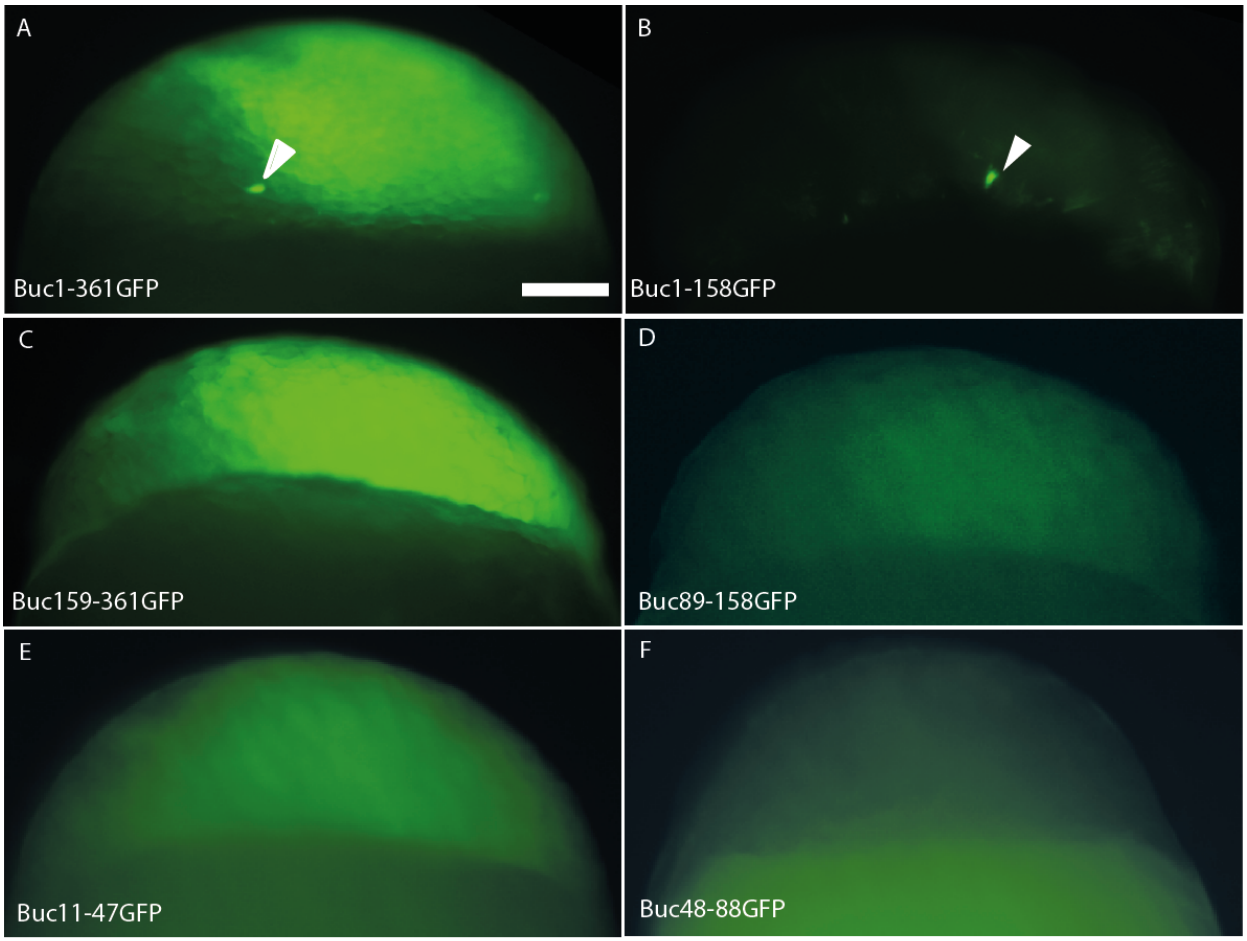

Fig. S5. Systematic mapping of Buc localization motif.

(A) N-terminal fragment of Buc (aa1-361) (white arrowhead) (100%). (B) Buc1-158 localizes (white arrowhead) (100%). (C) Buc159-361 is ubiquitous (0%). (D) Buc89-158 is ubiquitous (0%). (E) Buc11-47 is ubiquitous (0%). (F) Buc48-88 is ubiquitous (6.0±6.7%). Scale bar: 50 μm

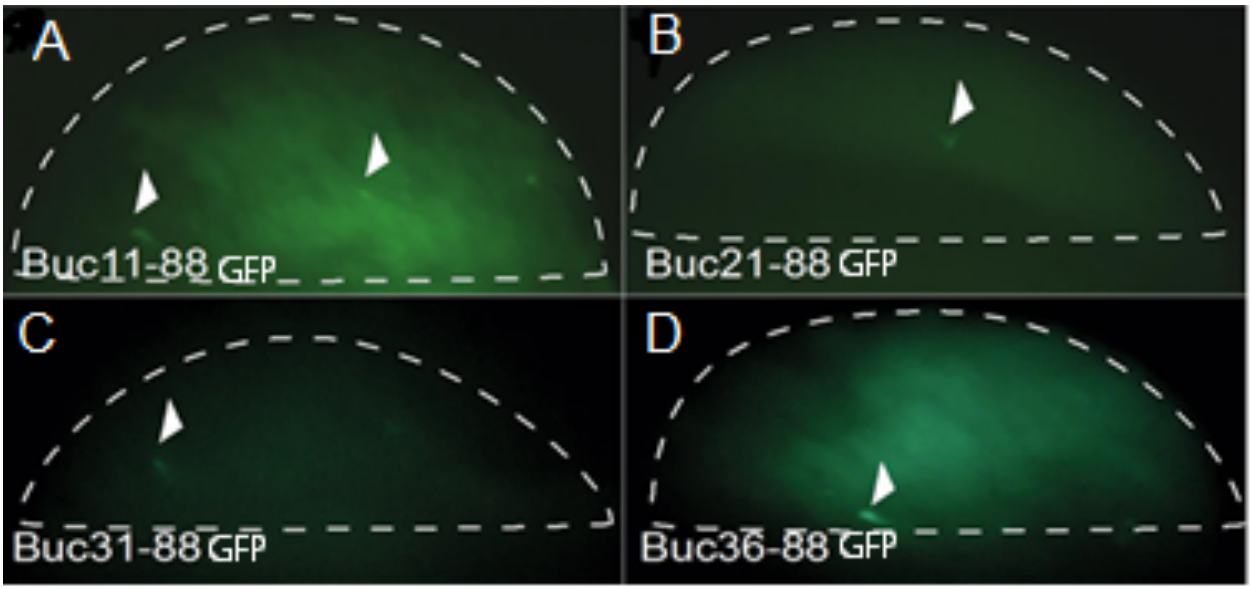

Fig. S6. Aggregation and localization of BucLoc are separate activities.
(A-D) Show embryos at high stage from the lateral view. Embryos are outlined by the dashed white line. Injected constructs showed fluorescent aggregates (white arrowheads). (A) Buc11-88 (91.4±6.8%). (B) Buc21-88 (67±4.0%). (C) Buc31-88 (60.1±7.9%). (D) Buc36-88 (52.2±13).

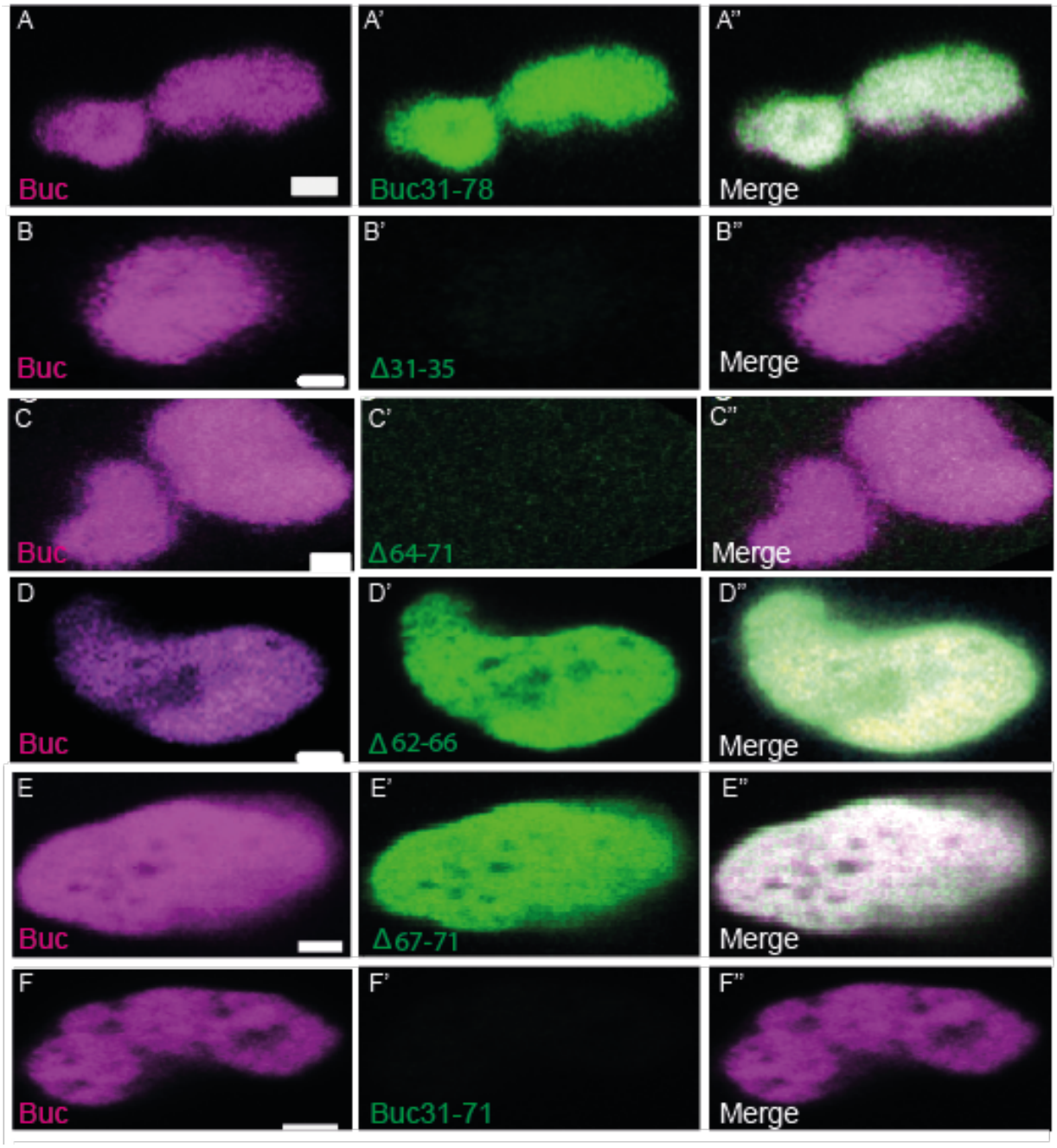

Fig. S7. Colocalization of deletion constructs of BucLoc mapping in Figure 5 with Buc-GFP. (A-A'') shows colocalization of transgenic Buc-GFP (magenta) and BucLoc-m-cherry fusion (aa31-78) (green). (B-B'') Shows colocalization of transgenic Buc-GFP (magenta) and Buc31-78 (Δ 31-35)-m-cherry fusion (green). (C-C'') Shows colocalization of transgenic Buc-GFP (magenta) and Buc31-78 (Δ 64-71)-m-cherry fusion (green). (D-D'') Shows colocalization of transgenic Buc-GFP (magenta) and Buc31-78 (Δ 62-66)-m-cherry fusion (green). (E-E'') Shows colocalization of transgenic Buc-GFP (magenta) and Buc31-78 (Δ67-71)-m-cherry fusion (green). (F-F'') Shows colocalization of transgenic Buc-GFP (magenta) and Buc31-71-m-cherry fusion (green). Embryos were injected at 1-cell stage with RNA encoding BucLoc-m-cherry fusions and imaged at high stage. The pictures are representing magnified germ plasm spots. Scale bars: 2 µm.

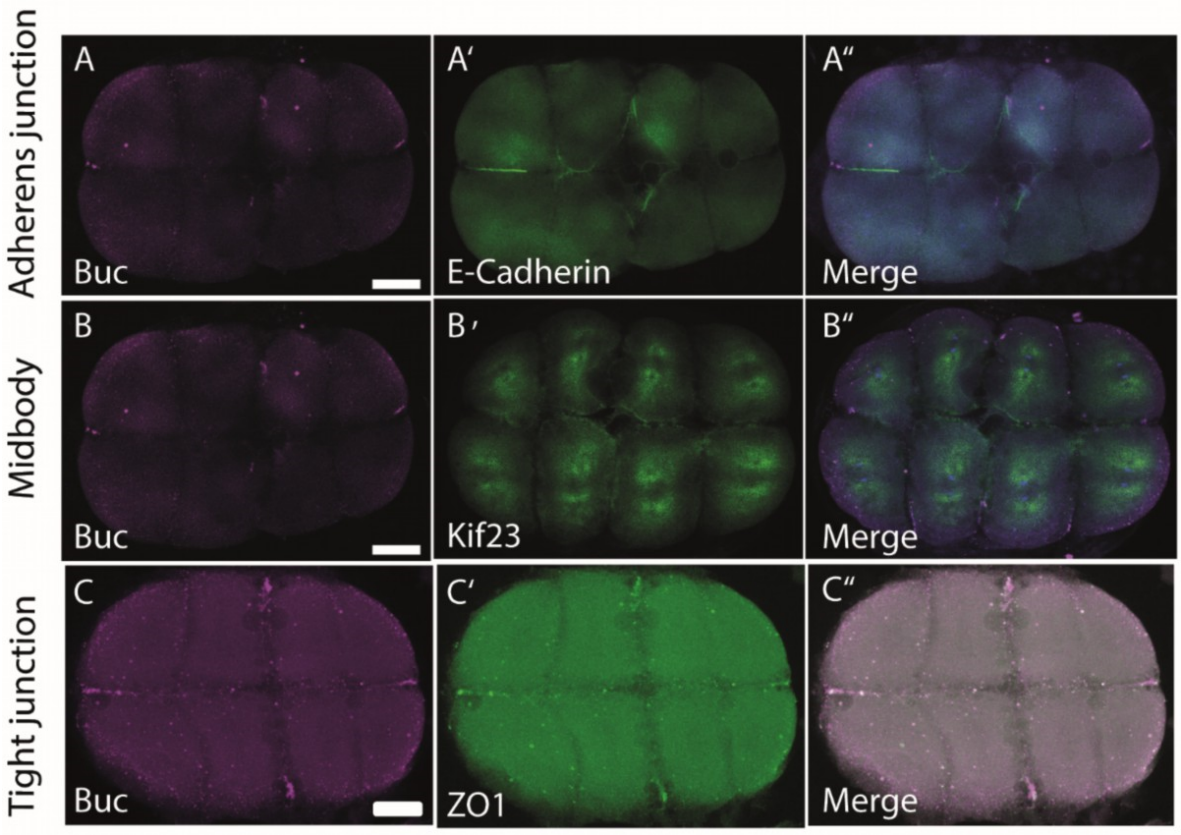

Fig. S8. Tight junction protein ZO1 colocalizes with Buc.

Colocalization analysis of Buc with different cellular structure markers. (A, B, C) Show animal view of immunostained 8-cell stage embryos 1st column - Buc (magenta), 2nd column – respective cellular structure (green), 3rd column – merge. (A-A‘‘) Immunostaining for Buc and adherens junction marker E-cadherin; (B-B‘‘) Buc and midbody marker Kif23; (C-C‘‘) Buc and tight junction marker Zonula occludens 1 (ZO1). Scale bars: 50 µm.

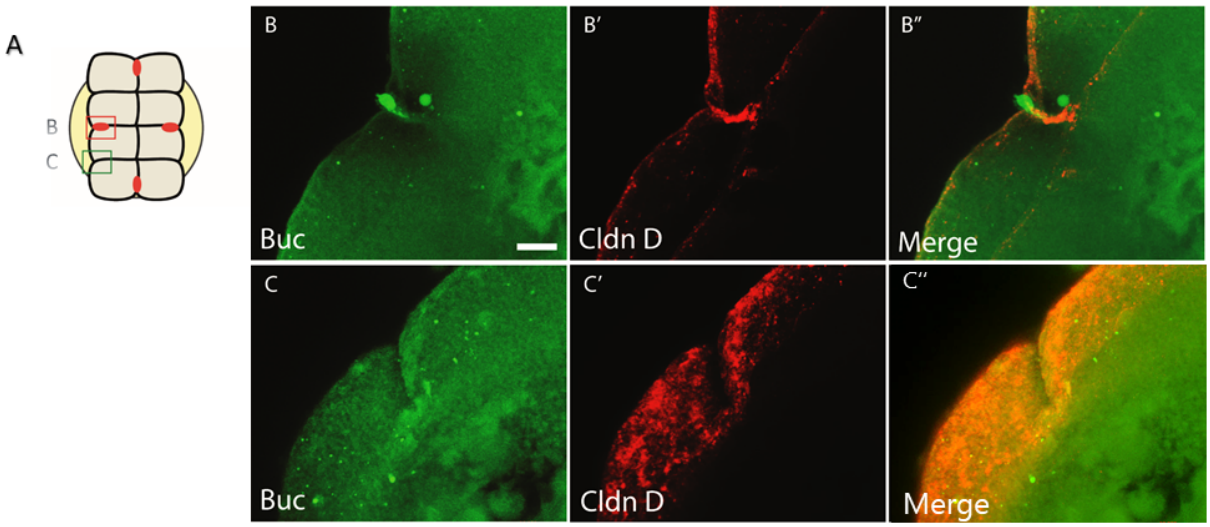

Fig. S9. Immunostaining shows overlap of Buc and *cldn-d*.

Zebrafish embryo at 8- cell stage was double stained with Buc and Cldn-d antibodies and their colocalization was analysed using confocal microscopy. A) A representative cartoon showing an embryo at 8- cell stage. (B-B'') Colocalization of Buc and Cldn-d at the middle cleavage furrow (the upper red rectangle in A). (C-C'') Localization of Buc and Cldn-d at the lower cleavage furrow (the lower green rectangle in A). Scale bar: 10 µm.

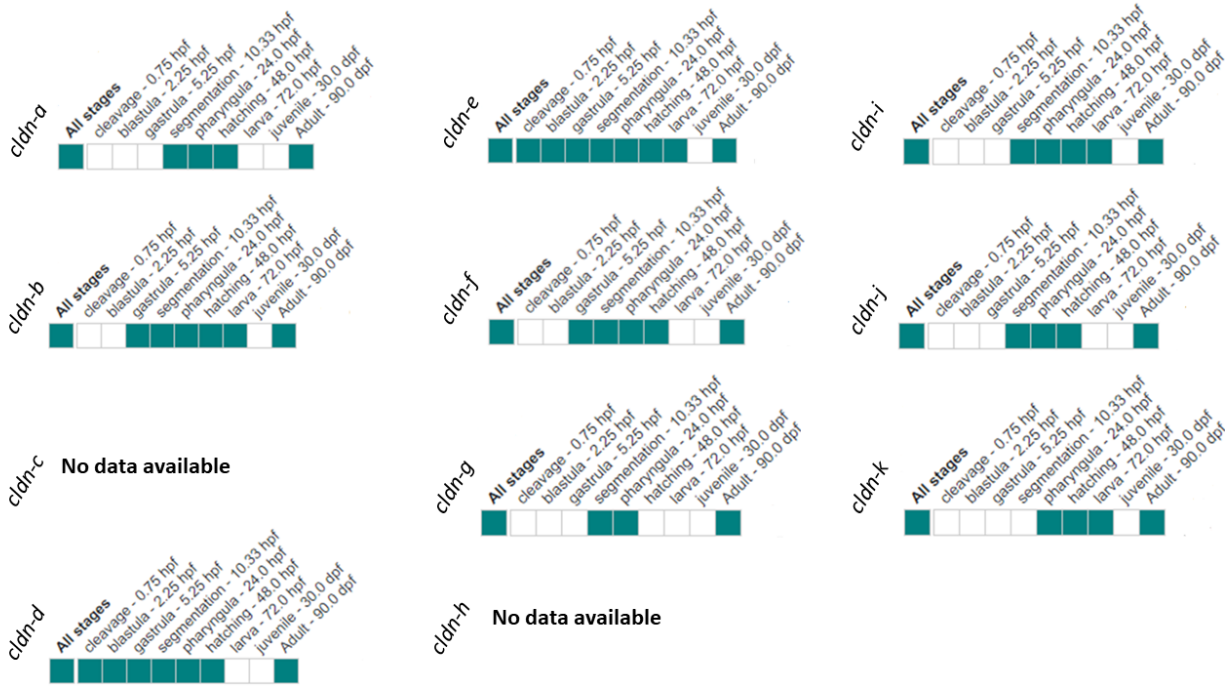

Fig. S10. Expression data of zebrafish cldns available on https://zfin.org/.

Expression of cldns at different developmental stages is shown in zebrafish. The green boxes represent annotated expression and the white boxes show no expression. Note only cldn-d and cldn-e showed expression at early developmental stages. The data is updated as on (date February 28th, 2021).

Table S1. 213 BucLoc interaction candidates selected from 3464 proteins identified by mass spectrometry analysis.

Identified Protein	Accession Number	GFP Co-IP	Buc-GFP Co-IP	BucLoc-GFP Co-IP
PREDICTED: protein PRRC2C [Danio rerio]	gi|528511146	79.6	1278.6	817.9
PREDICTED: zinc finger protein 318-like isoform X1 [Danio rerio]	gi|528497145	12.4	666.7	512.8
Cluster of PREDICTED: protein PRRC2B isoform X4 [Danio rerio] (gi|528481247)	gi|528481247 [2]	22.6	480.1	320.0
large proline-rich protein BAT2 [Danio rerio]	gi|319738640 (+2)	71.6	362.1	280.0
PREDICTED: msx2-interacting protein isoform X1 [Danio rerio]	gi|326678004 (+2)	63.3	434.0	257.4
PREDICTED: microtubule-actin cross-linking factor 1, isoforms 1/2/3/5 isoform X1 [Danio rerio]	gi|528510265	0.0	546.5	218.8
uncharacterized protein LOC792544 [Danio rerio]	gi|194353937	15.8	83.1	201.9
Cluster of PREDICTED: OTU domain-containing protein 4 isoformX1 [Danio rerio] (gi|528518829)	gi|528518829 [2]	83.8	417.6	189.9
PREDICTED: YLP motif-containing protein 1 isoform X2 [Danio rerio]	gi|528511017	36.9	232.6	185.5
PREDICTED: symplekin isoform X2 [Danio rerio]	gi|326668188 (+1)	52.9	218.7	184.5
PREDICTED: microtubule-associated protein futsch-like [Danio rerio]	gi|528497151	1.7	123.8	181.0
retinoblastoma-binding protein 6 isoform 1 [Danio rerio]	gi|302632528 (+4)	13.0	75.0	159.1
Cluster of PREDICTED: membrane-associated guanylate kinase, WW and PDZ domain-containing protein 1 [Danio rerio] (gi|528488944)	gi|528488944 [4]	62.6	191.7	157.7

guanine nucleotide-binding protein subunit beta-2-like 1 [Danio rerio]	gi|18859301	53.1	208.3	149.1
PREDICTED: uncharacterized protein LOC767754 isoform X1 [Danio rerio]	gi|528467168 (+2)	45.1	104.3	134.7
Cluster of eukaryotic translation initiation factor 4A, isoform 1A [Danio rerio] (gi|38198643)	gi|38198643 [3]	43.2	230.2	127.8
PERQ amino acid-rich with GYF domain-containing protein 2 [Danio rerio]	gi|71834468	55.0	261.2	123.5
Cluster of zinc finger CCCH domain-containing protein 13 [Danio rerio] (gi|319738618)	gi|319738618	39.2	118.6	120.6
Cluster of PREDICTED: cell cycle associated protein 1b isoform X1 [Danio rerio] (gi|528508316)	gi|528508316 [3]	39.1	262.3	117.6
Cluster of PREDICTED: eukaryotic translation initiation factor 4E transporter isoform X1 [Danio rerio] (gi|528482894)	gi|528482894 [2]	6.5	204.5	114.7
PREDICTED: cytoskeleton-associated protein 5 isoform X1 [Danio rerio]	gi|528520895	2.9	71.0	110.6
regulation of nuclear pre-mRNA domain containing 2a [Danio rerio]	gi|41053979	0.0	65.7	96.8
Cluster of LIM domain only 7b [Danio rerio] (gi|319996634)	gi|319996634 [2]	5.5	182.2	89.9
GPI-anchored membrane protein 1 [Danio rerio]	gi|51011059	17.0	206.9	89.8
PREDICTED: trinucleotide repeat-containing gene 6B protein [Danio rerio]	gi|528495941	0.0	130.1	84.6
Cluster of glutathione S-transferase pi [Danio rerio] (gi|18858197)	gi|18858197	7.1	32.3	82.7
Cluster of PREDICTED: pyrroline-5-carboxylate reductase isoform X1 [Danio rerio] (gi|528495079)	gi|528495079 [2]	28.1	108.1	81.0
ATP synthase subunit O, mitochondrial [Danio rerio]	gi|51467909	4.7	21.0	76.8
pre-mRNA cleavage complex 2 protein Pcf11 [Danio rerio]	gi|55925534	0.9	100.4	75.3

PREDICTED: DNA-directed RNA polymerase II subunit RPB1 isoform X2 [Danio rerio]	gi|528496057 (+1)	0.0	58.5	72.8
Cluster of ataxin-2 [Danio rerio] (gi|190358425)	gi|190358425 [2]	30.9	149.0	70.6
5'-3' exoribonuclease 1 [Danio rerio]	gi|289577074 (+1)	1.4	114.6	65.5
voltage-dependent anion-selective channel protein 2 [Danio rerio]	gi|41054601 (+1)	16.5	33.7	65.5
Cluster of splicing factor 45 [Danio rerio] (gi|41055474)	gi|41055474 [2]	13.5	132.2	57.6
voltage-dependent anion-selective channel protein 1 [Danio rerio]	gi|47777306	17.5	42.1	57.0
PREDICTED: protein FAM208A [Danio rerio]	gi|528517763	1.9	70.5	54.5
single-stranded DNA-binding protein, mitochondrial [Danio rerio]	gi|62955585	11.5	24.0	54.4
PREDICTED: tyrosine 3-monooxygenase/tryptophan 5-monooxygenase activation protein, zeta polypeptide isoform X1 [Danio rerio]	gi|528509453	3.6	13.6	53.7
non-POU domain-containing octamer-binding protein [Danio rerio]	gi|42415509	23.4	96.3	52.9
Cluster of PREDICTED: fish-egg lectin isoform X1 [Danio rerio] (gi|528491480)	gi|528491480 [5]	7.2	64.2	52.2
alpha-2-macroglobulin-like precursor [Danio rerio]	gi|320118891	0.0	17.3	50.3
Cluster of PREDICTED: chromodomain helicase DNA binding protein 4 isoform X1 [Danio rerio] (gi|528509046)	gi|528509046 [4]	1.7	30.1	49.5
14-3-3 protein epsilon [Danio rerio]	gi|47086819	4.6	12.4	47.8
Cluster of uncharacterized protein LOC100141336 precursor [Danio rerio] (gi|168823478)	gi|168823478 [5]	11.2	41.2	47.5
PREDICTED: protein SCAF11 isoform X1 [Danio rerio]	gi|528475676 (+2)	0.9	52.1	45.5
PREDICTED: cytoplasmic dynein 2 heavy chain 1-like, partial [Danio rerio]	gi|528502710	20.8	42.4	44.2

Cluster of PREDICTED: pericentriolar material 1 protein isoform X7 [Danio rerio] (gi|528467744)	gi|528467744 [3]	1.7	12.9	44.1
alpha-2-macroglobulin-like [Danio rerio]	gi|319655740 (+2)	2.9	18.7	43.1
PREDICTED: ubiquitin carboxyl-terminal hydrolase 10 isoformX1 [Danio rerio]	gi|326669691	1.0	138.2	42.9
PREDICTED: cleavage stimulation factor subunit 2-like isoform X1 [Danio rerio]	gi|326673799	11.3	86.7	40.3
Cluster of PREDICTED: alpha-2-macroglobulin isoformX1 [Danio rerio] (gi|326665588)	gi|326665588 [2]	8.9	60.0	39.8
PREDICTED: eukaryotic translation initiation factor 4 gamma 3 [Danio rerio]	gi|528517986	3.0	151.5	39.8
Ndufa9 protein [Danio rerio]	gi|157423514 (+2)	9.6	22.4	39.6
Zgc:158157 protein [Danio rerio]	gi|55250357	0.0	63.4	39.5
Cluster of myosin light chain alkali, smooth-muscle isoform [Danio rerio] (gi|47174755)	gi|47174755 [6]	8.7	17.3	39.1
Cluster of PREDICTED: uncharacterized protein LOC100000125 isoform X2 [Danio rerio] (gi|528510415)	gi|528510415 [3]	6.1	103.3	38.8
signal-induced proliferation-associated 1-like protein 1 [Danio rerio]	gi|529250122	2.8	31.4	38.7
eukaryotic translation initiation factor 4E-1B [Danio rerio]	gi|18858611	11.8	92.6	37.4
Cyc1 protein [Danio rerio]	gi|51327354 (+1)	11.5	32.9	35.8
complement component 1 Q subcomponent-binding protein, mitochondrial [Danio rerio]	gi|324021711 (+1)	9.0	19.2	35.8
LOC449616 protein [Danio rerio]	gi|213624848 (+2)	0.0	92.5	35.8
PREDICTED: cyclin-dependent kinase 13 [Danio rerio]	gi|326679472	5.8	67.7	33.7
Cluster of CWF19-like protein 2 [Danio rerio] (gi|76253886)	gi|76253886 [2]	0.0	28.5	32.6
nanog homeobox [Danio rerio]	gi|528505177 (+1)	3.9	60.8	32.4

PREDICTED: zinc finger CCCH domain-containing protein 4-like isoform X1 [Danio rerio]	gi|528501822	0.0	18.3	31.6
Cluster of PREDICTED: unconventional myosin-Va [Danio rerio] (gi|326680074)	gi|326680074 [4]	3.7	20.9	31.4
PREDICTED: protein FAM208A-like [Danio rerio]	gi|528516938	0.0	23.0	31.2
glutamate dehydrogenase 1b [Danio rerio]	gi|41282194	0.0	27.4	31.0
S-phase kinase-associated protein 1 [Danio rerio]	gi|41152201	14.5	29.8	30.8
PREDICTED: tyrosine-protein phosphatase non-receptor type 13 isoform X1 [Danio rerio]	gi|528513092 (+4)	6.4	107.4	30.7
Cluster of ADP-ribosylation factor 1 like [Danio rerio] (gi|41393117)	gi|41393117 [2]	0.0	11.2	30.1
Si:dkey-16k6.1 protein [Danio rerio]	gi|45767805 (+1)	2.4	7.8	29.8
Cluster of ras homolog gene family, member Ad [Danio rerio] (gi|50539958)	gi|50539958 [3]	1.2	16.1	29.4
tight junction protein ZO-2 isoform 1 [Danio rerio]	gi|320118869 (+2)	0.0	13.5	29.2
Cluster of uncharacterized protein LOC569235 precursor [Danio rerio] (gi|350536793)	gi|350536793 [3]	13.0	42.7	29.2
ATP-dependent RNA helicase DDX42 [Danio rerio]	gi|302318882	0.0	73.3	27.9
Cluster of PREDICTED: hypothetical protein LOC565404 [Danio rerio] (gi|189517232)	gi|189517232 [5]	6.7	58.2	27.5
PREDICTED: telomerase-binding protein EST1A-like isoform X1 [Danio rerio]	gi|326671361 (+1)	0.0	90.3	27.4
PREDICTED: ATP synthase subunit b, mitochondrial isoform X1 [Danio rerio]	gi|528487650 (+1)	3.5	9.1	27.1
mitochondrial import inner membrane translocase subunit Tim13 [Danio rerio]	gi|50539998	0.0	10.2	26.9
PREDICTED: RNA-binding protein 27 isoform X2 [Danio rerio]	gi|528491090 (+1)	5.8	32.9	26.7
PREDICTED: nudC domain-containing protein 1 isoform X1 [Danio rerio]	gi|528509803	2.7	11.2	26.6

regulation of nuclear pre-mRNA domain-containing protein 1B [Danio rerio]	gi|41054665 (+3)	0.0	63.3	25.4
nuclear pore complex protein Nup133 [Danio rerio]	gi|47087231	0.0	8.9	25.1
PREDICTED: RNA-binding protein 6 isoform X1 [Danio rerio]	gi|528483145	0.0	25.4	24.6
Cluster of PREDICTED: RNA-binding protein 26 [Danio rerio] (gi|528481486)	gi|528481486 [2]	2.5	30.2	24.6
glutamate dehydrogenase 1a [Danio rerio]	gi|47086875	0.0	11.1	24.5
Cluster of Bub3 protein [Danio rerio] (gi|53734038)	gi|53734038 [2]	3.2	16.2	23.8
Cluster of PREDICTED: cat eye syndrome critical region protein 2 isoform X2 [Danio rerio] (gi|528521383)	gi|528521383 [2]	0.0	46.3	23.6
LYR motif-containing protein 4 [Danio rerio]	gi|256000753	0.0	7.7	23.4
mitochondrial inner membrane protein [Danio rerio]	gi|47777298 (+1)	3.5	15.4	22.5
Abcf2 protein [Danio rerio]	gi|42542861 (+1)	7.3	27.2	22.5
DNA-directed RNA polymerase II subunit RPB2 [Danio rerio]	gi|302488402	0.0	33.2	22.5
Cluster of SNW domain-containing protein 1 [Danio rerio] (gi|50838798)	gi|50838798	7.9	39.3	22.4
PREDICTED: NFX1-type zinc finger-containing protein 1-like [Danio rerio]	gi|528483584	5.8	39.3	22.4
periphilin-1 [Danio rerio]	gi|121583944 (+1)	1.4	33.7	22.3
PREDICTED: unconventional myosin-IXa isoform X1 [Danio rerio]	gi|528486090 (+1)	0.0	56.0	22.2
PREDICTED: histone-lysine N-methyltransferase SETD1A isoform X1 [Danio rerio]	gi|326666050	0.0	38.1	21.9
PREDICTED: death-inducer obliterator 1-like [Danio rerio]	gi|528516988	0.0	59.7	21.9
Cluster of LOC100000597 protein [Danio rerio] (gi|66910514)	gi|66910514 [5]	0.0	10.2	21.7
dolichyl-diphosphooligosaccharide--	gi|154426290	0.0	10.2	21.1

protein glycosyltransferase subunit DAD1 [Danio rerio]				
protein QIL1 [Danio rerio]	gi|113678245	4.2	10.2	21.1
PREDICTED: E3 ubiquitin-protein ligase TTC3 isoform X2 [Danio rerio]	gi|528491184	2.8	70.6	21.0
serine/threonine-protein phosphatase 2A 56 kDa regulatory subunit delta isoform [Danio rerio]	gi|50726892	0.0	5.5	20.9
cytochrome b-c1 complex subunit Rieske, mitochondrial [Danio rerio]	gi|157073897	0.0	6.1	20.7
Cluster of Protein regulator of cytokinesis 1 [Danio rerio] (gi|28279644)	gi|28279644 [2]	7.5	61.7	20.4
PREDICTED: E3 ubiquitin-protein ligase HERC2, partial [Danio rerio]	gi|528483182	0.0	8.5	20.0
Cluster of LOC563225 protein [Danio rerio] (gi|115292012)	gi|115292012 [2]	7.9	17.8	19.7
Cluster of eukaryotic translation initiation factor 4B [Danio rerio] (gi|47550837)	gi|47550837 [6]	0.0	41.9	19.6
high mobility group protein B2 [Danio rerio]	gi|82658290	0.9	5.7	19.4
Icln protein [Danio rerio]	gi|44890532 (+2)	7.6	23.6	19.3
nuclear pore complex protein Nup160 [Danio rerio]	gi|41054908	0.0	5.3	19.3
Cluster of TNF receptor-associated protein 1 [Danio rerio] (gi|165972373)	gi|165972373 [2]	0.0	71.3	18.8
Cluster of PREDICTED: microtubule-associated serine/threonine-protein kinase 3-like [Danio rerio] (gi|528470977)	gi|528470977 [2]	0.0	25.5	18.8
M-phase phosphoprotein 8 [Danio rerio]	gi|187607764	2.4	42.2	18.7
PREDICTED: PHD finger protein 3 isoform X1 [Danio rerio]	gi|528498598 (+1)	0.0	18.4	18.5
PREDICTED: sideroflexin-3 isoform X1 [Danio rerio]	gi|528497698	1.9	7.2	18.2
Cluster of Epithelial cell adhesion molecule [Danio rerio] (gi|44890710)	gi|44890710 [2]	1.8	13.9	18.0
Sept2 protein [Danio rerio]	gi|115313325 (+3)	0.0	13.3	17.6

Cluster of PREDICTED: regulation of nuclear pre-mRNA domain-containing protein 2 isoform X1 [Danio rerio] (gi|528502856)	gi|528502856 [2]	0.0	12.6	17.5
Zgc:77560 protein [Danio rerio]	gi|42542976 (+1)	2.4	66.6	17.4
Cluster of PREDICTED: nucleolar pre-ribosomal-associated protein 1-like [Danio rerio] (gi|528501168)	gi|528501168 [2]	2.9	20.9	17.3
ras-related protein Rab-14 [Danio rerio]	gi|41393147	0.0	5.1	16.8
NADH dehydrogenase [ubiquinone] 1 beta subcomplex subunit 10 [Danio rerio]	gi|41152268	3.5	17.2	16.8
Cluster of oxoglutarate (alpha-ketoglutarate) dehydrogenase (lipoamide) [Danio rerio] (gi|254028264)	gi|254028264 [2]	0.0	5.6	16.6
Pard3 protein [Danio rerio]	gi|190339230 (+4)	0.9	32.3	16.6
DNA-directed RNA polymerase II subunit RPB3 [Danio rerio]	gi|269784633	0.0	22.8	16.3
RecName: Full=Protein CASC3; AltName: Full=Cancer susceptibility candidate gene 3 protein homolog; AltName: Full=Metastatic lymph node protein 51 homolog; Short=DrMLN51; Short=Protein MLN 51 homolog	gi|123886565 (+1)	6.3	28.9	16.1
Cluster of serine/threonine kinase 36 (fused homolog, Drosophila) [Danio rerio] (gi|320043268)	gi|320043268	6.0	13.9	16.0
cytotoxic granule-associated RNA binding protein 1 [Danio rerio]	gi|47086779	6.4	16.9	16.0
Cluster of PREDICTED: uncharacterized protein LOC393431 isoform X1 [Danio rerio] (gi|528486792)	gi|528486792	0.0	9.1	16.0
Cluster of nuclear receptor corepressor 2 [Danio rerio] (gi|380420327)	gi|380420327 [4]	0.0	57.7	15.9
Cas-Br-M (murine) ecotropic retroviral transforming sequence-like 1 [Danio rerio]	gi|41055074	3.3	20.8	15.7

PREDICTED: polyribonucleotide 5'-hydroxyl-kinase Clp1-like [Danio rerio]	gi|189528302	0.0	53.2	15.4
uncharacterized protein LOC556124 [Danio rerio]	gi|157909776	1.4	30.5	15.2
succinate dehydrogenase [ubiquinone] iron-sulfur subunit, mitochondrial precursor [Danio rerio]	gi|148922926	5.4	11.3	14.9
Cluster of cAMP-dependent protein kinase catalytic subunit alpha [Danio rerio] (gi|130493522)	gi|130493522 [3]	0.0	8.8	14.9
serine/threonine-protein kinase 3 [Danio rerio]	gi|41054445 (+1)	3.6	49.0	14.8
uncharacterized protein LOC541537 [Danio rerio]	gi|62122901	0.0	7.4	14.6
chromodomain-helicase-DNA-binding protein 8 [Danio rerio]	gi|320461545 (+2)	0.0	22.7	14.6
PREDICTED: splicing factor, arginine/serine-rich 15 [Danio rerio]	gi|528492333	0.0	20.4	14.4
zinc finger HIT domain-containing protein 3 [Danio rerio]	gi|41053670	3.5	33.1	14.0
eukaryotic translation initiation factor 6 [Danio rerio]	gi|41055624 (+2)	0.0	9.1	13.9
PREDICTED: nuclear pore complex protein Nup153 isoform X1 [Danio rerio]	gi|528510621	0.0	17.5	13.7
PREDICTED: uncharacterized protein LOC436879 isoform X4 [Danio rerio]	gi|528517594	0.0	11.1	13.3
Zgc:111960 protein [Danio rerio]	gi|166796880	0.0	11.6	13.2
very low-density lipoprotein receptor precursor [Danio rerio]	gi|169646705 (+4)	0.0	5.1	13.0
C-terminal binding protein 1 [Danio rerio]	gi|40254690	3.3	11.6	12.9
claudin-like protein ZF-A89 [Danio rerio]	gi|30725822	0.0	5.2	12.8
Cluster of PREDICTED: C2 domain-containing protein 3 [Danio rerio] (gi|528501432)	gi|528501432	0.0	9.2	12.7
PREDICTED: histone deacetylase 1 isoform X1 [Danio rerio]	gi|528510099	2.6	29.6	12.0
peptidyl-prolyl cis-trans isomerase-like 1 [Danio rerio]	gi|77683061	1.9	18.6	11.9

Cluster of ras-related C3 botulinum toxin substrate 1 [Danio rerio] (gi|54792776)	gi|54792776 [2]	3.5	11.7	11.9
PREDICTED: uncharacterized protein KIAA0556-like [Danio rerio]	gi|528520519	0.0	14.9	11.8
PREDICTED: trinucleotide repeat-containing gene 6B protein-like isoform X2 [Danio rerio]	gi|528472879 (+1)	0.0	23.4	11.7
nuclear pore complex protein Nup107 [Danio rerio]	gi|71834480	1.8	6.9	11.3
Cluster of PREDICTED: tight junction protein ZO-1-like [Danio rerio] (gi|528521995)	gi|528521995	0.0	12.5	11.3
DIS3-like exonuclease 1 [Danio rerio]	gi|160333118	0.0	32.6	11.3
PREDICTED: PAB-dependent poly(A)-specific ribonuclease subunit 2-like isoform X2 [Danio rerio]	gi|528518391 (+1)	0.0	13.3	11.2
Cluster of PREDICTED: PERQ amino acid-rich with GYF domain-containing protein 1-like isoform X1 [Danio rerio] (gi|528492127)	gi|528492127 [2]	0.0	13.3	11.2
uncharacterized protein LOC550263 [Danio rerio]	gi|62955177	0.0	14.9	11.2
Cluster of PREDICTED: serine/threonine-protein kinase TAO2-like [Danio rerio] (gi|125812164)	gi|125812164	0.0	17.9	10.7
PREDICTED: uncharacterized protein LOC503771 isoform X3 [Danio rerio]	gi|528519733	0.0	17.1	10.6
Cluster of LOC559853 protein, partial [Danio rerio] (gi|79151969)	gi|79151969 [2]	0.0	38.9	10.4
PREDICTED: serine/threonine-protein kinase LATS1 isoform X1 [Danio rerio]	gi|528510786	0.0	20.4	10.2
PREDICTED: cyclin-dependent kinase 12 [Danio rerio]	gi|528509066	0.9	29.5	10.0
poly(rC)-binding protein 2 [Danio rerio]	gi|41055221	0.0	12.7	9.9
nanog homeobox [Danio rerio]	gi|148357118	0.0	28.5	9.9
Cluster of TIA1 cytotoxic granule-associated RNA binding protein [Danio rerio] (gi|37681959)	gi|37681959 [4]	4.8	33.1	9.9

protein mago nashi homolog [Danio rerio]	gi|62955377	3.8	15.8	9.8
nucleoporin 98 [Danio rerio]	gi|320118905 (+1)	0.0	7.5	9.7
uncharacterized protein LOC100126100 precursor [Danio rerio]	gi|157954446 (+1)	2.9	22.5	9.7
N-acetyltransferase 10 [Danio rerio]	gi|41055301	4.7	15.0	9.7
OCIA domain-containing protein 1 [Danio rerio]	gi|41053513 (+1)	0.0	5.8	9.5
cytochrome c oxidase subunit II [Danio rerio]	gi|8395615	2.4	5.1	9.5
PREDICTED: transcription factor 19 [Danio rerio]	gi|292624089	0.0	17.6	9.4
signal recognition particle 9 [Danio rerio]	gi|41055367	0.0	5.1	9.4
actin related protein 2/3 complex subunit 4 [Danio rerio]	gi|45387521	0.0	7.4	9.1
PREDICTED: lysine-specific demethylase 6A isoform X1 [Danio rerio]	gi|528490350 (+1)	0.0	26.6	8.8
exosome complex exonuclease RRP4 [Danio rerio]	gi|339717151	2.9	22.8	8.8
PREDICTED: bromodomain adjacent to zinc finger domain, 2A isoform X1 [Danio rerio]	gi|528517226 (+1)	0.0	8.0	8.7
PREDICTED: AF4/FMR2 family member 4 isoform X1 [Danio rerio]	gi|528514500 (+3)	2.6	13.3	8.6
Cluster of PREDICTED: kinesin family member 13A [Danio rerio] (gi|528505240)	gi|528505240 [5]	0.0	5.4	8.4
exosome complex exonuclease RRP45 [Danio rerio]	gi|54400656	0.0	20.2	8.4
exosome complex component MTR3 [Danio rerio]	gi|66472734	1.0	14.4	8.1
MGC174638 protein [Danio rerio]	gi|156230391 (+2)	0.0	7.8	8.0
Cluster of cyclin-L1 [Danio rerio] (gi|41054323)	gi|41054323	3.6	13.3	7.7
Xrcc5 protein [Danio rerio]	gi|133777834	0.0	12.9	7.7
sorting and assembly machinery component 50 homolog B [Danio rerio]	gi|55925219	0.0	5.2	7.4

Cluster of PREDICTED: rho GTPase-activating protein 21 isoform X1 [Danio rerio] (gi|528470502)	gi|528470502 [2]	0.0	10.9	7.4
60S ribosomal protein L29 [Danio rerio]	gi|51010951	2.9	11.6	7.1
immediate early response 3-interacting protein 1 precursor [Danio rerio]	gi|356991159	0.0	5.1	7.0
transmembrane and coiled-coil domains 1 [Danio rerio]	gi|50540216 (+1)	1.9	8.7	7.0
PREDICTED: wu:fc48e01 [Danio rerio]	gi|125820176	0.0	18.4	6.8
Zgc:123096 protein, partial [Danio rerio]	gi|50417024 (+1)	0.0	6.1	6.6
PREDICTED: protein TANC1-like isoform X2 [Danio rerio]	gi|528481904 (+1)	0.0	9.1	6.4
Centrin2 [Danio rerio]	gi|161213715 (+1)	1.9	14.9	6.3
PREDICTED: dehydrogenase/reductase SDR family member 7B isoform X1 [Danio rerio]	gi|528473478	0.0	10.8	6.3
cyclin T2b [Danio rerio]	gi|47086855	2.7	16.8	6.3
U4/U6.U5 tri-snRNP-associated protein 1 [Danio rerio]	gi|50540414	0.0	15.6	5.9
PREDICTED: uveal autoantigen with coiled-coil domains and ankyrin repeats [Danio rerio]	gi|292616084 (+1)	0.0	6.6	5.9
C-Myc-binding protein [Danio rerio]	gi|91176306	0.0	15.4	5.9
transcription elongation factor B polypeptide 1 [Danio rerio]	gi|52219182 (+1)	0.0	7.7	5.9
Cluster of cytochrome c oxidase assembly factor 5 [Danio rerio] (gi|238859533)	gi|238859533	0.0	5.1	5.9
PREDICTED: uncharacterized protein DKFZp762I1415-like [Danio rerio]	gi|68399071	0.0	5.1	5.9
Ku70 autoantigen [Danio rerio]	gi|114215700 (+2)	1.6	7.4	5.7
uncharacterized protein LOC100216070 [Xenopus (Silurana) tropicalis]	gi|213983243 (+1)	0.0	11.3	5.6
RNA-binding protein 8A [Danio rerio]	gi|61651846	2.4	9.0	5.6

G kinase anchoring protein 1 [Danio rerio]	gi|32451811 (+3)	0.0	17.8	5.6
PREDICTED: nuclear receptor coactivator 3 [Danio rerio]	gi|326671802	0.0	14.8	5.3
Cluster of PREDICTED: mps one binder kinase activator-like 1B-like [Danio rerio] (gi|292614396)	gi|292614396 [5]	0.0	9.1	5.1
coiled-coil-helix-coiled-coil-helix domain-containing protein 2, mitochondrial [Danio rerio]	gi|41152140	0.0	8.1	5.1
store-operated calcium entry-associated regulatory factor precursor [Danio rerio]	gi|115495791 (+2)	0.0	13.2	5.0

Table S2. Data for 16-cell injection assay.

Cldn-dΔYV	***R1***	***R2***	***R3***	***R4***
total	38	20	20	16
same	21	8	12	9
down	10	10	6	7

uninejcted	***R1***	***R2***	***R3***	***R4***
total		20	21	16
same		18	20	16
down		0	0	0

Cldn-d	**R1**	**R2**	**R3**	**R4**	
total		20	16	13	
same		19	8	13	
down		0	3		0

R: Replicate total: total number of embryos same: embryos did not lose germ plasm spot down: embryos lost a germ plasm spot

Note: Buc spots were counted twice in each embryo, right after injection (16 cell stage) and at 2 hpf.

Table S3. Cloned constructs.

Insert	Vector	Cloning method	FW Primer	RV Primer	Note
buc-egfp	pCS2+	-	-	-	Bontems et al., 2009.
sosk	pCS2+	restriction enzyme cloning	TTGTTCTTTTTGCAGGATCATGACCATCATCGAGAGCAAC	TCGAATCGATGGGATCGTGGTATGTTCTCCAGGGACGG	
sOsk	pDONR221	Gateway	GGGGACAAGTTTGTACAAAAAAGAGGCTATATGACCATCATCGAG AGCAAC	GGGGACCACTTTGTACAAGAAAG CTGGGTAGTGGTATGTTCTCCAGGGACGG	pENTR221 was recombined with pCSDest2 and p3EeGFP to produce pEXPpCSDest2.
buc1-361	pDONR221	Gateway	GGGGACAAGTTTGTACAAAAAAGCAGGCTCTATGGAAGGAATAAATAACAATTCA	GGGGACCACTTTGTACAAGAAAG CTGGGTTGCTGTAGGAATAAGCACTGCC	pENTR221 was recombined with pCSDest2 and p3EeGFP to produce pEXPpCSDest2.
buc1-158	pDONR221	Gateway	GGGGACAAGTTTGTACAAAAAAGCAGGCTCTATGGAAGGAATAAATAACAATTCA	GGGGACCACTTTGTACAAGAAAG CTGGGTTAGGGGTAGAAGAGACTACATTGTT	pENTR221 was recombined with pCSDest2 and p3EeGFP to produce pEXPpCSDest2.
buc159-361	pDONR221	Gateway	GGGGACAAGTTTGTACAAAAAAGCAGGCTCTATGGATGTGGTGCAGGGAGAGAA	GGGGACCACTTTGTACAAGAAAG CTGGGTTGCTGTAGGAATAAGCACTGCC	pENTR221 was recombined with pCSDest2 and p3EeGFP to produce pEXPpCSDest2.
buc11-88	pDONR221	Gateway	GGGGACAAGTTTGTACAAAAAAGCAGGCTATATGGGAGTTGGGCAACCTCA	GGGGACCACTTTGTACAAGAAAG CTGGGTATCTTCTGTAATCAATTGGCTG	pENTR221 was recombined with pCSDest2 and p3EeGFP or p3EmCherry to produce pEXPpCSDest2.
buc89-158	pDONR221	Gateway	GGGGACAAGTTTGTACAAAAAAGCAGGCTTAATGATTAACCCCACTACCCCTC	GGGGACCACTTTGTACAAGAAAG CTGGGTTAGGGGTAGAAGAGACTACATTGTT	pENTR221 was recombined with pCSDest2 and p3EeGFP to produce pEXPpCSDest2.
buc11-47	pDONR221	Gateway	GGGGACAAGTTTGTACAAAAAAGCAGGCTTAATGGGAGTTGGGCAACCTCA	GGGGACCACTTTGTACAAGAAAG CTGGGTAGCCATATGGATTCATGGGCC	pENTR221 was recombined with pCSDest2 and p3EeGFP to produce pEXPpCSDest2.
buc48-88-	pDONR221	Gateway	GGGGACAAGTTTGTACAAAAAAGCAGGCTTAATGGAGTGTGCTGTGAAAACTG	GGGGACCACTTTGTACAAGAAAG CTGGGTATCTTCTGTAATCAATTGGCT	pENTR221 was recombined with pCSDest2 and p3EeGFP to produce pEXPpCSDest2.
bucΔ11-88-egfp	pCS2^{+}		buc_265bp_fw: ATTAACCCCCACTACCCCTCAGT buc_1bp_wo-loc_fw: ATGGAAGGAATAAATAACAATTCACAACCAATTAACCCCCACTACCCCTCAGTTGCATCC Buc_1bp_ClaI_fw: GGGATCGATATGGAAGGAATAAATAACAATTCAC	eGFP_end_XbaI_rv: GGGTCTAGATTACTTGTACAGCTCGTCCATGC	*bucΔ11-88-egfp*sequence was amplified using a 3-step PCR from pCS2+ buc-eGFP, using the primers buc_265bp_fw, buc_1bp_wo-loc_fw, Buc_1bp_ClaI_fw, eGFP_end_XbaI_rv. The PCR product was cut with ClaI, XbaI and ligated into pCS2+.
buc21-88-GFP		Gateway	GGGGACAAGTTTGTACAAAAAAGCAGGCTATATGCCACCATCTCAGCCTTATTT	GGGGACCACTTTGTACAAGAAAG CTGGGTATCTTCTGTAATCAATTGGCTG	pENTR221 was recombined with pCSDest2 and p3EmCherry to produce pEXPpCSDest2.
Buc36-88-GFP				GGGGACCACTTTGTACAAGAAAG CTGGGTATCTTCTGTAATCAATTGGCTG	pENTR221 was recombined with pCSDest2 and p3EmCherry to produce pEXPpCSDest2.

buc31-78-mCherry		Gateway	GGGGACAAGTTTGTACAAAAAAGCAGGCTATATGCCACCATCTCAG CCT	GGGGACCACTTTGTACAAGAAAG CTGGGTAATGTGGAATCACATAGCC	pENTR221 was recombined with pCSDest2 and p3EmCherry to produce pEXPpCSDest2.
buc31-78(Δ31-35)mCherry		Gateway	GGGGACAAGTTTGTACAAAAAAGCAGGCTATATGTATTTCATGTATC AGTGG	GGGGACCACTTTGTACAAGAAAG CTGGGTAATGTGGAATCACATAGCC	pENTR221 was recombined with pCSDest2 and p3EmCherry to produce pEXPpCSDest2.
Buc31-78(Δ31-35)mCherry		Oligo + Gateway	Oligo: ATGTATTTCATGTATCAGTGGCCCATGAATCCAATGGCCATTACGGTTTTCCCGGGCCGGCTTTGCACTTTGGCCGTCCCTAT		buc31-78-Δ31-35 was amplified using the primers Buc31-78_Δ31-35_fw_gateway, Buc31-78_rev_gateway from the extended overlapping oligos: Buc31-78_Δ31-35_fw and Buc_57-78_rev. The PCR product was recombined into pDONR221.
Buc31-78(62-66)mCherry		Oligo + Gateway		Oligo: ATGTGGAATCACATAGCCAGGATACTGCATAAACTGGGGACGGCCAAAGTGCAAAGCCGGCCCGGGAAAACCGTAATGGCCATATGG	buc31-78-Δ62-66 was amplified using the primers Buc31-78 _fw_gateway, Buc31-78_rev_gateway from the extended overlapping oligos: BucLoc_Δ62- 66_rev, Buc_31-51_fw. The PCR product was recombined into pDONR221
Buc31-78(67-71)mCherry		Oligo + Gateway		Oligo: ATGTGGAATCACATAGCCAGGATAAGGGGCCATATAGGGACGGCCAAAGTGCAAAGCCGGCCCGGGAAAACCGTAATGGCCATATGG	buc31-78-Δ67-71 was amplified using the primers Buc31-78 _fw_gateway, Buc31-78_rev_gateway from the extended overlapping oligos: BucLoc_Δ67- 71_rev, Buc_31-51_fw. The PCR product was recombined into pDONR221
Cldn-d		Gateway	GGGGACAAGTTTGTACAAAAAAGCAGGCTTAATGGCATCTGTTGGGCTTCAG	GGGGACCACTTTGTACAAGAAAGCTGGGTTTCACACATAAGCTCCTGGAGCAG	pENTR221 was recombined with pCSDest2 to produce pEXPpCSDest2.
Cldn-a		Gateway	GGGGACAAGTTTGTACAAAAAAGCAGGCTTAATGGTATCAGCAGGGCTGCAG	GGGGACCACTTTGTACAAGAAAGCTGGGTTTCAGACATACCCCTTGGTTCCTC	pENTR221 was recombined with pCSDest2 and p3EmCherry to produce pEXPpCSDest2.
Cldn-dΔYV		Gateway	GGGGACAAGTTTGTACAAAAAAGCAGGCTTAATGGCATCTGTTGGGCTTCAG	GGGGACCACTTTGTACAAGAAAGCTGGGTTTTAAGCTCCTGGAGCAGACCT	pENTR221 was recombined with pCSDest2 and p3EmCherry to produce pEXPpCSDest2.

Table S4. A full list of the 3464 proteins identified by mass spectrometry

Click here to download Table S4

Table S5. Antibodies used for immunostaining

Antibody	Dilution
Guinea pig-α-Buc (Biogenes, Berlin)	1:5000
Mouse-α-B-catenin (Merck, Kenilworth, USA)	1:1000
Mouse-α-E-cadherin (BD Transduction Laboratories, Franklin Lakes, New Jersey, USA)	1:50
Rabbit-α-p-NMII (Cell Signaling Technology, Danvers, USA)	1:50
Mouse-α-Kif23 (Gene Tex, Irvine, California, USA)	1:50
Rat-α-ZO1 (Santa Cruz Biotechnology, Dallas, Texas, USA)	1:100
Rabbit -α-DDX4 (Bioss, USA)	1:300
Goat-α-guinea pig Alexa Fluor 488 (Life Technologies, Carlsbad, USA)	1:500
Goat-α-rabbit Alexa Fluor 594 (Life Technologies, Carlsbad, USA)	1500
Cldn-d	1:25

Table S6. Antibodies used for western blotting

Antibody	Dilution
Guinea pig-α-Buc (BioGenes, Berlin)	1:5000
Mouse-α-GFP (Merck, Kenilworth, USA)	1:2500
Goat-α-guinea pig 800CW (IRDye, Li-Cor)	1:20,000
Goat-α-mouse 680CW(IRDye, Li-Cor)	1:20,000